# A physics-based rock-friction constitutive law, part I: steady-state friction.

Einat Aharonov[1] & Christopher H. Scholz[2]

1) Institute of Earth Sciences, The Hebrew University, Jerusalem, 91904, Israel
2) Lamont-Doherty Earth Observatory of Columbia University, Palisades, New York, USA

**Key points:**

1) A physics-based model is derived for steady-state friction of rocks, using microphysics of asperity contact creep.
2) Assuming thermal & mechanical steady-state, we generalize steady-state rate & state friction for all slip rates, elucidating its physics.
3) Using independently-determined material parameters, the model predicts experimentally observed quartz/granite friction at all slip rates.

## Abstract

Experiments measuring friction over a wide range of sliding velocities find that the value of the friction coefficient varies widely: friction is high and behaves according to the rate and state constitutive law during slow sliding, yet markedly weakens as the sliding velocity approaches seismic slip speeds. We introduce a physics-based theory to explain this behavior. Using conventional microphysics of creep, we calculate the steady-state velocity and temperature dependence of contact stresses during sliding, including the thermal effects of shear heating. Contacts are assumed to reach a coupled thermal and mechanical steady-state, and friction is calculated for steady sliding. Results from theory provide good quantitative agreement with reported experimental results for quartz and granite friction over 12 orders of magnitude in velocity. The new model elucidates the physics of friction and predicts the connection between friction laws and independently determined material parameters. In this paper we show that the theory fits well low confining stress and room temperatures experiments. In a companion paper in this issue the same theory is used to model high temperature experiments.

## 1) Introduction

The physics controlling frictional resistance during sliding between surfaces has been intensely studied for centuries. It is of particular importance to earthquake physics, as the relation between friction and shearing velocity controls stability of sliding on geological faults and earthquake nucleation, location and size *(e.g. Scholz, 1998).* Thus, previous work concentrated on the relation between friction and velocity and between friction and temperature (for reviews see *Marone 1998; Scholz, 2002*). Experimental observations on many geologic materials show that at low slip velocities friction is high (~0.6-0.8) and has only a second order dependence on velocity. Above a critical velocity friction falls precipitously, as shown in Fig 1 *(DiToro et al, 2011).* At intermediate velocities there may be a peak in friction for some materials *(Spagnuolo et al, 2016),* as also seen in Fig 1. In addition, friction is observed to change as a function of ambient temperature in all materials (e.g. *Blanpied et al 1995, Lockner et al 1986, Chester 1994, Van Diggelen et al 2010, Verberne et al 2015, Chester and Higgs 1992).* An important challenge is to combine all these observations into a coherent, physics-based, description of friction as function of the full range of velocity, from slow to very fast, varying normal stress up to a few hundred of MPa and varying ambient temperature up to the brittle ductile transition. This is basic for understanding earthquake physics, assessing stability of faults, and predicting the brittle-ductile transition in the earth *(e.g. Marone and Scholz 1988, Scholz 1988, 1998).*

### i. Previous Work on the Physics of Friction – micromechanics of contacts

In their classic series of works on friction, *Bowden and Tabor (1964)* suggested that the friction coefficient, $\mu$, measured macroscopically as the ratio of shear to normal stress applied to the surface during sliding, $\mu = \sigma_n / \tau$, actually reflects some averaging of the physical interactions that occur among a multitude of interacting microscopic contacts during sliding (Fig 2a). Bowden and Tabor (abbreviated here as B&T) suggested that the *real area of contact* between surfaces, $A_r$, is much smaller than the apparent area of the surface, $A$, and is given by $\sigma_c A_r = W$, where $W$ is the normal load and $\sigma_c$ is the indentation hardness of the material. Thus each contact is under a much higher normal stress than the nominal stress $\sigma_n$, and the contact stress is $\sigma_c = \sigma_n A/A_r$. If the contacts require a specific shear stress, $\tau_c$, for yielding in shear, then the shear force needed to shear the surface is $F=\tau_c A_r$, and the coefficient of friction becomes $\mu = F/W = \tau_c/\sigma_c$. This idea, of existence and yielding of microscopic contacts as the origin of macroscopic friction, is one of the pillars of present day understanding of dry friction *(e.g. Stachowiak & Batchelor 2013).*

It is by now well established *(e.g. Dieterich & Kilgore 1994, Rubenstein et al 2004)* that indeed shearing surfaces touch at a sparse array of contacts (Fig 2a), that at room temperature constitute < 1% of the apparent area, $A$. The main issue is finding the appropriate expressions for $\tau_c$ and $\sigma_c$, as these are not simply constant values of plastic yield stresses, as initially was assumed. One demonstration of the non-constancy of contact stresses comes from the observation *(Dietrich & Kilgore 1994)* that the real contact area, $A_r$, grows logarithmically with time of contact, so that $\sigma_c$ decays logarithmically with contact time. Indeed, static friction, the resistance to initiate sliding from rest, is measured to increase logarithmically with contact time *(Dieterich 1972).* Another demonstration for the non-constancy of $\sigma_c$ & $\tau_c$ is the observed variation of friction with slip rate and temperature *(e.g. Blanpied et al 1995, Chester and Higgs 1992).*

### ii. Previous Work on the Physics of Friction – Rate and State theory

In addition to the contact-yielding concept of B&T, the empirically-based Rate and State *(R/S)* theory was developed to model observations on friction, that showed that the macroscopic steady-state friction, $\mu_{ss}$, depends logarithmically on slip rate V *(Scholz et al, 1972)* and on hold time in stationary contacts *(Dieterich, 1972).* The R/S friction law, in its several variations *(Dieterich 1979, Ruina 1983)* now thirty years old, sparked a revolution in earthquake physics. It allowed us the ability to understand frictional instability in terms of a small number of empirical friction parameters that could be readily measured in the laboratory. From this the gamut of earthquake behavior could be deduced (e.g. *Scholz, 1998).* For *steady-state* sliding R/S can be written as (e.g. *Scholz, 1998)*

$$(1) \qquad \tau = \sigma_n \mu = \sigma_n \left[\mu^* + (a-b) \ln(V/V^*)\right]$$

The constants $\mu^*$ & $V^*$ are often chosen arbitrarily in R/S literature, and the constant pre-factors $a$ and $b$ are viewed as defining linearization about steady-state. In this framework, the relative values of $a$ and $b$ control stability of sliding, and therefore are suggested to control earthquake nucleation *(Dieterich 1978, Scholz 1998).* Eqn (1) was shown by many experiments to provide a good description of sliding friction at slow velocities (e.g. see reviews in *Marone 1998; Baumberger & Caroli 2006).*

R/S is very different in concept from B&T theory, as it was developed as a constitutive empirical relation without considering the physics of contacts. Yet, although the $ln(V/V_*)$ term in eq (1) was introduced empirically by *Dieterich (1979,1978)* and *Ruina (1983),* many studies suggest that it arises from thermally activated creep processes at asperity contacts (e.g. *Chester 1994, Heslot et al. 1994, Brechet & Estrin 1994, Baumberger 1997, Nakatani 2001, Rice et al, 2001, Baumberger & Caroli 2006, Noda 2008, Putelat et al 2011).* Since at room temperature real contact area is typically <1% of the nominal area (e.g. *Dieterich & Kilgore 1994, Rubenstein et al 2004),* assuming 10MPa applied normal stress, each contact experiences stress of the order of 1GPa. At such high stress, creep is expected to be exponential in stress, and may proceed by one or several of the following physio-chemical mechanisms: stress corrosion, leading to subcritical crack growth *(Atkinson, 1987)* and static fatigue *(Scholz, 1972);* Peierls-type mechanisms impeding dislocation glide *(Evans & Goetze 1979, Tsenn &Carter 1986, Rice et al 2001),* and solution transfer creep (pressure solution) *(Nakatani & Scholz 2004a,b).* In friction there are two components of creep that must be considered: normal creep that shortens the contact and increases its area, and creep on contact surfaces that accommodates shear sliding (Fig 2b). Thermally activated creep in both these components was used to explain/predict the observed R/S behaviors, for both slow (e.g. *Brechet and Estrin 1994; Nakatani 2001, Nakatani & Scholz 2004a,b, Baumberger & Caroli 2006)* and intermediate rate sliding *(Bar Sinai et al, 2014, Noda 2008).*

### iii. Recent Work on the Physics of Friction – high slip rate

A different behavior from the R/S logarithmic behavior occurs at high slip rate. Using new high-speed experimental apparatuses, a dramatic weakening was observed at all sliding materials (Fig 1) at around V~O($10^{-2}$) m/s, independent of material (e.g. *DiToro et al 2004, 2011; Han et al 2007, 2010; Del Gaudio et al., 2009; Hirose & Bystricky, 2007; Nielsen et al., 2008; Mizoguchi et al., 2007; Ferri et al., 2010; De Paola et al. 2011; Fondriest et al 2013; SimanTov et al 2015; Boneh et al 2013; Proctor et al 2014).* This high-velocity weakening has been attributed to a variety of mechanisms, all of them related to shear-heating:

1) “Flash heating” of highly–stressed, short-lived, contact asperities. Heated contacts soften and weaken, and even melt at high V (e.g. *Yao et al 2016; Goldsby & Tullis 2011; Rice 2006; Beeler et al 2008).*

2) Chemical/phase changes: e.g. decomposition in carbonates (e.g. *Sulem & Famin 2009; Goren et al 2010),* or Silica gel formation in quartz (e.g. *Goldsby & Tullis 2002, Kirckpatrick et al 2013).*

3) Thermal pressurization due to shear heating of pore fluids *(e.g. Rice 2006; Ferri et al 2010; Goren & Aharonov 2007, 2009, 2011; Faulkner et al., 2011; Noda & Lapusta, 2013).*

4) Localization and thermo-elastic instabilities *(e.g. Braeck and Podladchikov, 2007; Kelemen and Hirth, 2007; SimanTov et al 2015; Platt et al 2014; Brown and Fialko, 2012),* possibly also driven by decomposition *(Platt et al, 2015).*

5) Special behavior of nano-grain layers, that often cover principle slip-zones in faults (e.g. *Green et al 2014, Verberne et al 2014a,b, De Paola et al 2015, Chen et al 2013, Reches & Lockner 2010, SimanTov et al 2013, 2015).*

Much of the above mentioned work (as well as other work) on high V sliding have been quite successful in explaining steady-state friction as function of velocity. Yet nearly always these studies allowed fitting of free parameters, and so didn’t involve full constraint by material parameters. In addition, none of the above works was able to carry the physics from low to high V, and from low to high ambient temperature and normal stress. They all looked at some window of the velocity, normal stress and temperature phase space.

To summarize the current state of affairs in theoretical understanding of rock friction: separate theories exist for slow and fast shearing, many based on the Bowden and Tabor concept, and many are fitted somewhat freely. To the best of our knowledge, there is currently no unifying, physics-based model, which may be applied to different minerals, to predict friction across velocities and ambient temperatures. Such a model is needed to predict sliding stability of faults (e.g. *Scholz 1998, Noda & Lupsta 2013)* and the brittle-ductile transition (e.g. *Shimamoto & Noda 2014*).

### iv. This work

The R/S friction laws, being empirical, were rather opaque, lending themselves to various interpretations of the physical processes represented by earthquake behavior and their relationships with the parameters in the laws. It was naively hoped that the friction parameters would be dependent only on the material, so that measurements of these for a few key fault-forming minerals would map out the seismogenic nature of faults in various environments. Laboratory measurements now show that the steady-state friction parameters, even for a given mineral type, vary in complex ways with sliding velocity, temperature, normal stress and with the microstructure formed on the fault sliding surfaces (e.g. *den Hartog et al 2012; Verberne et al 2014a,b, 2015; Blanpied et al 1995; Chester and Higgs 1992; Carpenter et al, 2016).*

These developments make it clear that for further progress to be made a physics-based friction law that incorporates the R/S friction elements needs to be developed. Here we present some basic steps in that direction. We present a single, physics-based, friction law to explain friction observations in rocks, across a wide range of rock types, slip velocities and temperatures, predicting the data in Fig 1 and similar experimental findings. Our theory models friction at all velocities continuously, from low to high contact temperature regimes, connecting previously proposed physics of contact creep at low contact temperature, to flash heating at intermediate contact temperature, and to flash melting/decomposition at high contact temperature. Although our model is general, we apply our results first to quartz and granite, as these materials have currently the largest number of friction data. Also, most of the thermodynamic parameters that appear in our formulation of the friction law can be estimated from independent measurements for quartz. Hence for quartz-rich rocks we can make quantitative and independent comparisons of theory with friction experiments, rather than relaying on data fitting.

Specifically, we show below that our model may explain and predict the following general observations that are not material specific:

A. High friction and 2nd order material-dependent V-dependence at low V. (R/S friction law behavior).

B. Material independent abrupt thermally induced velocity-weakening above a critical V.

C. Material dependent peak at intermediate V.

D. All material dependencies result from independently determined variations in material properties.

In addition, we will show in a companion paper, Paper 2, that using the same parameters that were used here for the low T and low normal stress experiments, we may model steady-state quartz and granite friction at high T and high normal stress.

## 2) Theory

### i. Assumption 1: Friction arises from creep of contacts, and is predictable from contact stresses.

We follow B&T, assuming friction arises from interactions of highly-stressed contacts of microscopic asperities between surfaces or grains. The contacts exhibit time-dependent shortening and spreading under the applied normal load, so that the asperity height *h* shortens with time via thermally activated creep driven by the normal stress on the contact, $\sigma_c$. Since plasticity maintains volume, their contact area grows as they shorten, thereby reducing the contact stress $\sigma_c$. In a similar manner, shearing is assumed to occur at a rate V via thermally-activated shear creep, driven by the shear stress on contacts, $\tau_c$. This formalism for the physics of friction has been extensively developed over the last decades (e.g. *Heslot et al. 1994, Brechet & Estrin 1994, Nakatani 2001, Rice et al, 2001, Baumberger & Caroli 2006, Putelat et al 2011).* Creep is assumed to be exponential in contact stresses $\tau_c$ and $\sigma_c$ (e.g. *Chester 1994, Evans & Goetze 1979, Tsenn & Carter 1986).* Thermal activation depends on contact temperature, $T_c$, and uses the general expression for exponential creep based on rate theory *(e.g., Poirier, 1985).* Under these assumptions, the equations for the shearing velocity *V* and contact (asperity) compaction (or convergence) velocity, *dh/dt*, are:

$$\text{(2a)} \qquad V = V_{smax} \exp(-\frac{Q_s - \tau_c N \Omega_s}{R T_c});$$

$$\text{(2b)} \qquad \frac{dh}{dt} = -V_{nmax} \exp(-\frac{Q_v - \sigma_c N \Omega_v}{R T_c});$$

*N* is Avogadro number, *R* the gas constant, and *h* is the asperity height. $V_{smax}$ and $V_{nmax}$ are reference, (highest possible), shear and normal creep rates, achieved when contact stresses are at their highest possible value $\tau_c = \tau_c^* = Q_s/N\Omega_s$ and $\sigma_c = \sigma_c^* = Q_v/N\Omega_v$, respectively. Note that if $\tau_c > \tau_c^*$ or $\sigma_c > \sigma_c^*$, the physics in eqn (2) breaks down and a different physics must control contact deformation. Eqn (2) describes thermally activated creep in which the deformation is controlled by thermally activated jumps dictated by a pinning potential field with valley depth Q (activation energy) and spacing of valleys of the order of $\Omega^{1/3}$ (activation volume). Eqns (2a) & (2b) are basically eqns 6 & 12 of Putelat et al (2011), respectively. It is important to note that activation energy, $Q_s$, and activation volume, $\Omega_s$, for surface creep, may differ from bulk volumetric creep parameters, $Q_v$ and $\Omega_v$, as depicted in Fig 2b. The potentially different values of activation energies and volumes for shear and normal creep will be discussed further below and shown by our results to be very important in controlling both the absolute value of the friction coefficient, and its velocity dependence.

Although eqns (2a) and (2b) are symmetrical, the two dependencies of $\sigma_c$ & $\tau_c$ on shear velocity *V* are different. This difference is due to the different boundary conditions in the normal and tangential directions: while steady-state sliding experiments impose the shear velocity *V* as a boundary condition, the convergence rate *dh/dt* is not imposed. Its temporal evolution is solved from equation (2b). To solve eqn (2b), we assume that contacts in steady state sliding are created and destroyed continuously. Steady state entails that each contact has a lifetime that depends on sliding rate *V* and contact size *d*. For each contact the moment it is born is t=0, at which time the height of the contact is $h_0$, its radius $r_0$, and the normal stress on it $\sigma_c^0$. Following *Brechet & Estrin (1994), Baumberger & Caroli (2006)* and *Putelat et al (2011),* we assume constant contact volume during plastic deformation, i.e. $r^2h=r_0^2h_0$, where *r* is contact radius at any time *t*. For steady-state sliding we assume constant number of equal sized contacts, *n,* per unit area, so $\sigma_N A = \sigma_c A_r = \sigma_c n\pi r^2$. Thus $\sigma_c = \sigma_c^0 h/h_0$ and $d\sigma_c/dt = (\sigma_c^0/h_0)\, dh/dt$. From these, eqn (2b) may be rewritten as

$$\text{(2c)}\qquad \frac{d\sigma_c}{dt} = -V_{nmax}\frac{\sigma_c^0}{h_0}\exp\left(-\frac{Q_v-\sigma_c N\Omega_v}{RT_c}\right);$$

We can now integrate the differential equation (2c) to calculate the contact stress, $\sigma_c(t)$, as function of time since formation of the contact, the thermodynamic variables, and the initial contact stress $\sigma_c^0$ at time of contact formation.

$$\text{(2d)}\qquad \sigma_c(t) = \sigma_c^0[1 - b'\ln(1 + t/t_c)];$$

$$(2e)\qquad b' = \frac{RT_c}{\sigma_c^0 N\Omega_v};\ \ t_c = b'\frac{h_0}{V_{nmax}}\exp\left(\frac{Q_v - N\Omega_v\sigma_c^0}{RT_c}\right)$$

The characteristic time constant, $t_c$, was defined as the “cutoff time” by *Berthoud et al, (1999)*, and its physical meaning will be discussed below in the Discussion.

In order to evaluate $\sigma_c$ (or *$A_r$),* the contact stress at time *$t=0$,* $\sigma_c^0$, is needed. $\sigma_c^0$ was previously assumed (Putelat et al ,2011) to be $\sigma_c^0 = \sigma_c^* = \frac{Q_v}{N\Omega_v}$, meaning that if the 'indentation hardness' was measured at time t=0, it would be equal to the highest possible stress for this process. However there are four main reasons to think that $\sigma_c^0 = B\frac{Q_v}{N\Omega_v}$, with $0<B<1$:

1. There is no physical argument that dictates that the two values- the 'indentation hardness' at time of contact initiation and the thermodynamic parameter $\frac{Q_v}{N\Omega_v}$, should be equal, and no reason to think contact stress is initially always at the value $\frac{Q_v}{N\Omega_v}$.
2. An assumption that $\sigma_c^0 = \frac{Q_v}{N\Omega_v}$ forces contact-normal creep rate (*dh/dt* in eqn 2b) at time t=0, to be independent of temperature, while it is reasonable to expect it to be thermally activated - to vanish at $T_c=0$ and increase to maximum rate, $V_{nmax}$, at $T_c \rightarrow \infty$. This argument leads to $0<B<1$.
3. The assumption of B=1 in eqn (2e) implies that the cutoff time $t_c$ is constant with $T_c$, and the activation energy for $t_c$, $E_c$, is 0. A factor $0<B<1$ dictates that $t_c$, the "cutoff time" for the logarithmic contact-area creep, is thermally activated, with an activation energy $E_{tc}=(1-B)Q_v$. In this case $t_c$ decreases with T, as measured by *Nakatani & Scholz (2004a)*. A non-zero activation energy is measured by their experiments (their fig 7), and serves as proof that B should be <1.
4. The indentation hardness at time t=0, $\sigma_c^0$, and thus also B, are expected to decrease with ambient temperature, following *Evans (1984),* who measured that indentation hardness of quartz drops by 30-50% as temperature is raised from 0 to 500°C. So not only is B < 1, it is even not a constant. Instead it drops with the ambient temperature $T_0$.

We now rewrite equation (2a-2d) doing two things- first inverting eqn (2a) to obtain $\tau_c$ as function of V, eqn (3b). Second, use the contact life time in steady-state sliding rate *t=d/V* (where *d=2r* is the contact diameter), in place of time in eqn (2d):

( 3a) $$\sigma_c(t) = \sigma_c^0\left(1 - b' \ln\left(1 + \frac{d}{Vt_c}\right)\right)$$

( 3b) $$\tau_c(t) = \tau_c^*(1 + a' \, ln\left(\frac{V}{V_{smax}}\right))$$

$$(3c)\qquad \frac{A_r}{A} = \frac{\sigma_N}{\sigma_c^0}\frac{1}{\left(1 - b'\ln\left(1 + \frac{d}{Vt_c}\right)\right)}$$

$$(3d)\qquad a' = \frac{RT_c}{Q_s};\ \ b' = \frac{RT_c}{BQ_v}\ ;\ \ \sigma_c^0 = \frac{Q_v B}{N\Omega_v};\ \ \tau_c^* = \frac{Q_s}{N\Omega_s};\ \ E_{tc}=Q_v - N\Omega_v\sigma_c^0\text{=(1-B)}Q_v$$

$$(3e)\qquad t_c = b'\frac{d}{V_{nmax}}\exp\left(\frac{E_{tc}}{RT_c}\right) = t_{cr}\frac{T_c}{T_{cr}}\exp(-\frac{E_{tc}\,\Delta T_c}{R\,T_c\,T_{cr}});$$

Eqns (3d-e) provide the constants for calculating contact stresses $\sigma_c$ and $\tau_c$ in eqns 3a-b. Eqn (3) is the same as in the above mentioned previous studies (see *Putelet et al (2011)* for detailed derivation, and *Nakatani and Scholz (2004b),* derivation of their eqn. 13), except for the newly added pre-factor *B,* that affects mainly $t_c$ and its activation energy, $E_{tc}$. Assuming a reference cutoff time $t_{cr}$ at a reference temperature $T_{cr}$, and $\Delta T_c = T_c - T_{cr}$, and dividing $t_c$ by this reference cutoff time $t_{cr}$, provides eqn(3e) as another formulation for the cutoff time, with more easily obtained parameters than those in eqn(2e). Note that the physics behind this formalism dictates that constants $V_{smax}$ & $V_{nmax}$ are much greater than the sliding rate *V,* as they represent the physical upper limit to the creep-rate in the respective creep processes.

Eqn (3c) provides the real contact area, calculated from eqn (3a) using $\sigma_N A = \sigma_c A_r$. The behavior predicted by (3c), namely logarithmic growth of real contact area with time, is observed in micro-indentation experiments by *Scholz and Engelder (1976)* in both Olivine and Quartz.

The friction coefficient is easily obtained from eqns (3) via

$$(4a)\mu_{ss} = \frac{\tau}{\sigma_n} = \frac{\tau_c}{\sigma_c}$$

The steady-state friction coefficient, $\mu_{ss}$, in eqn (4a) may be Taylor expanded, when the b’ term is much smaller than 1 in eqn (3a), to obtain:

$$(4b)\ \ \mu_{ss} \sim \mu_0\left\{1 + a'\ln\left(\frac{V}{V_{smax}}\right) + b'\ln\left(1 + \frac{d}{t_c V}\right)\right\}$$

$$= \mu_0 + a\ln\left(\frac{V}{V_{smax}}\right) + b\ln\left(1 + \frac{d}{t_c V}\right)$$

$$(4c)\ \ a = a'\mu_0 = \mu_0\frac{RT_c}{Q_s};\ \ b = b'\mu_0 = \mu_0\frac{RT_c}{BQ_v};\ \ \mu_0 = \frac{\tau_c^*}{\sigma_c^0} = \frac{Q_s}{BQ_V}\frac{\Omega_V}{\Omega_S}$$

Here $\sigma_n$ and $\tau$ are the applied normal and shear stress on the surface, and the variables $a', b', t_c$ are given by eqn (3d-e). Eqn (4b) is valid when the *b* term (not only the *b* pre-factor) is sufficiently smaller than 1 in eqn (3a). It is easy to calculate that the *b* term remains small under all realistic conditions: it is largest when either $V \rightarrow 0$ (which increases the absolute value of the $ln$ term) or when $T_c$ is high (which increases $b$). The coefficient $b'$ is of order 0.01 at room temperature (see Table 2), and grows to 5 times that value when $T_c$ is near melting, which is still very small. The $ln$ term is small as long as V fulfills the condition that $V >> \frac{d}{t_c} e^{-1/b'}$ which, using the parameters of Table 1, is seen to be easily met for any geological slip rate. For accuracy we calculate friction in our model directly from $\frac{\tau_c}{\sigma_c}$, i.e. from eqn (3) and not from eqn (4b), but the approximation of eqn (4b) is valid and therefore we use it below for analysis and explanation of frictional behaviors.

The equivalence between eqn (4b) and the R/S eqn (1), indicates that *a, b* and $V^*$ in R/S eq (1) are not arbitrary fitting constants, but instead represent material constants. These points are discussed at length in previous work *(e.g. Rice et al 2001, Noda 2008, Baumberger & Caroli 2006, Putelet et al 2011).*

As a consequence of eqn (4), contact temperature and friction are strongly coupled. During sliding, contact temperature, $T_c$, rises due to frictional shear-heating, which is controlled by the friction coefficient in eqn (4). On the other hand, rising $T_c$ changes frictional resistance via pre-factors *a, b* and $t_c$ in eqns (3) & (4). Thus $T_c$ and $\mu_{ss}$ are coupled, and this coupling is crucial in controlling intermediate to high-speed friction, as proven recently in the experiments of *Yao et al (2016).*

### ii. **Assumption 2: Steady-state temperature and friction.**

As seen in *DiToro et al (2011)* (their fig 1, here reproduced as fig 3), high velocity friction weakens with slip and reaches a steady-state after sliding a distances $D_{th}$. This high velocity weakening is thermally induced, by various mechanisms including (but not limited to) flash heating, decomposition in carbonates, melting in quartz, and thermal pressurization. All of those mechanisms require a steady frictional heat production to be maintained, which results in negative feedback such that steady-states in friction and temperature are simultaneously maintained.

To calculate the steady-state contact temperature, $T_c$, we follow previous formulations (e.g. *Rice 2006, Noda 2008, Beeler et al 2008),* and assume that sliding contacts undergo "flash heating", via shear heating that takes place during short "contact-life-times". Flash heating of contacts elevates $T_c$ by amount $\delta T$ above the average temperature of the surface, $T_s$, which also increases during sliding. Steady-state contact temperature $T_c$ is thus approximated by the sum of the mean surface temperature after sliding distance $D_{th}$ (eqn 1 in *DiToro et al, 2011*), $T_s = T_0 + \frac{\tau_c}{\rho C}\frac{\sigma_n}{\sigma_c}\sqrt{\frac{V D_{th}}{\pi\alpha}}$, plus flash heating contributions on contacts, $\delta T = \frac{\tau_c}{\rho C}\sqrt{\frac{Vd}{\pi\alpha}}$, (eqn (3) from *Rice 2006*), where $T_0$ is ambient temperature, α thermal diffusivity coefficient, C heat capacity, and ρ density of the material:

$$(5)\quad T_c = T_s + \delta T = T_0 + \frac{\tau_c}{\rho C}\sqrt{\frac{V}{\pi\alpha}}\left[\sqrt{d} + \frac{\sigma_n}{\sigma_c}\sqrt{D_{th}}\right]$$

At high enough sliding velocity, eqn (5) predicts contact temperatures $T_c$ that exceed the phase transition temperature of the particular mineral, in this case the melting temperature in quartz *($T_m$)*. Yet thermodynamic considerations predict that the temperature at the contacts will remain at the phase boundary, i.e. $T_c = T_m$, even if V increases. To maintain $T_c$ at $T_m$ with increasing V, eqn (5) predicts shear stress at contact must follow $\tau_c \sim 1/\sqrt{V}$, since

$$6)\ \tau_c^m(V) = \rho C\sqrt{\pi\alpha}(T_{melt} - T_0)/\left(\sqrt{V}\left[\sqrt{d_m} + \frac{\sigma_n}{\sigma_c^m}\sqrt{D_{th}}\right]\right)$$

where we assume $d_m$ & $\sigma_c^m$ are constant and independent of V.

## 3) Parameter values

To solve coupled eqns (3-5) (and also eqn (6) once melting sets on) we constrain values of the parameters used, via previous independent measurements. All of these parameters are thermodynamic or mechanical parameters of the mineral. Here we concentrate on the mineral quartz for which many of those parameters are well determined.

**Activation energies** $Q_v$, $Q_s$, values are constrained to within a factor of less than 2, which is not too bad given that the processes that control the creep are not well constrained. We expect a difference between $Q_v$ & $Q_s$: Shear deformation involves very high strain in a surface layer whereas the surface-normal deformation involves presumably a much smaller (volumetric) strain. These two processes may result in different defect structures, and especially the high dislocation density can result in strengthening of the surface layer. Additionally, these two processes may result in different interstitial water content which can greatly effect the activation energy of quartz *(Mainprice and Jaoule, 2009).* The variability of Q as function of water content was measured by *Mainprice & Jaoul (2009),* who found dislocation creep activation energy in quartzite ranged between 185 kJ mol−1 for vacuum dried to 151 kJ mol−1 for 0.4 wt% water added samples. Thus, activation energy for bulk deformation that controls normal creep, $Q_v$, and surface deformation that controls shear creep, $Q_s$, need not be equal. Activation energies cited previously in the literature do not distinguish between volume and surface processes, and do not even discuss the possibility for such difference. However here this difference is crucial as it will be shown later to determine the value of friction and its R/S behavior. Q associated with quartz friction usually ranges between 150 -250 KJ/mol (*Nakatani 2001, Rice et al 2001, Kirby & Kronenberg 1987, Mainprice and Jaoul, 2009)*, but values ranging between 90-500 KJ/mol have also been suggested *(Nakatani 2000).* Here we thus used values ranging between 150 - 250 KJ/mol based on the above citations.

Similarly, **volumetric and surface activation volumes**, $\Omega_v$ and $\Omega_s$ respectively, are not precisely known and need not necessarily be equal. They again are expected to reflect specific defect structures and process, but values have not been suggested in connection to any specific physical process. Activation volumes are of the size of atomic volumes. Estimates for Ω for quartz friction vary up to 50%, ranging between $(0.37\text{nm})^3=5*10^{-29}\text{m}^3$ *(Nakatani, 2001)* to $5\text{x}(0.25\text{nm})^3=7.8*10^{-29}\text{m}^3$ *(Rice et al 2001).*

To calculate **cutoff times** $t_c$ (eqn 3e), one needs either $V_{nmax}$ or a reference cutoff time, $t_{cr,}$ at a reference contact temperature, $T_{cr}$. $t_{cr}$ values have been experimentally measured, while there is little knowledge of $V_{nmax}$. Room temperature $t_{cr}$ were measured in experiments to range from 1 s *(Dieterich 1972,1978)* to 10,000 s *(Nakatani and Scholz, 2004a),* with the latter attributed to time scales of pressure solution. In addition, *Nakatani and Scholz (2004b),* measured $t_c$ as function of $T_0$, and found $t_c$ is thermally activated, with an **activation energy** in quartz of $E_{tc}$=58KJ/mol. We can use this measured $E_{tc}$ to constrain also the **prefactor B**: from eqn 3c, $E_{tc}=(1-B)Q_v$, so that assuming $Q_v=300KJ/mol$ and $E_{tc}=58KJ/mol$ gives $B\sim0.81$, while assuming $Q_v=170KJ/mol$ with this $E_{tc}$ gives $B\sim0.66$. These constraints on B should be used cautiously, due to the fact that this value of $E_{tc}$ was measured during pressure solution. $E_{tc}$ is probably different in the experiments that measured $t_{cr}\sim1s$, since the controlling process is different, but we don't know this for certain as $E_{tc}$ was not measured there.

An independent additional constraint on **prefactor *B*** comes from the value of **yield stress**, $\sigma_c^0=\frac{Q_v B}{N\Omega_v}$. Optical measurement of asperity contact sizes (*Dieterich & Kilgore, 1994,1996*) on various materials including soda-lime and quartz suggest that $\sigma_c^0 \sim 0.2G$, or even larger, where ***G* is shear modulus**. This value is consistent with an estimate by *Boitnott et al. (1992)* and with micro-hardness indentation strengths measured by *Dieterich & Kilgore (1994)* (as interpreted by *Rice et al (2001)).* Using $G=31GPa$ for quartz, this estimate suggests $\sigma_c^0$~6GPa, and using $Q_v$=250KJ/mol and $\Omega_v=5*10^{-29}m^3$ in $\sigma_c^0=\frac{Q_v B}{N\Omega_v}$ then predicts B~0.72. A lower activation energy, $Q_v$=170KJ/mol gives higher value for B, B>0.9. However, high B values and low $Q_v$ values would dictate a low $E_{tc}$<20KJ/mol (according to eqn 3e). We therefore use the following ranges: $Q_v=220\pm70$ KJ/mol and $B\sim0.85\pm0.1$, consistent with all experimental constrains known today for $E_{tc}$, $\sigma_c^0$, and $Q_v$. This constrains $E_{tc}$ to be between 10-75 KJ/mol.

The value of B quoted above is for room ambient temperature, yet $\sigma_c^0$ and B should be a function of $T_0$. *Evans (1984)* showed that indentation hardness of quartz, i.e. yield stress, drops by 30-50% as $T_0$ increases from 0 to 500C. To represent this effect we use $B(T_0)=B_r\exp(-0.0006(T_0-T_r))$, so that $\sigma_c^0$ drops with ambient temperature $T_0$ following the trend in fig 5 of *Evans (1984).*

Another parameter is the upper limit for shear rate, $\boldsymbol{V_{smax}}$. The maximum value of $V_{smax}$ has been equated to the natural vibration frequency of atoms in a mineral lattice, and linked to the shear wave velocity $c_s$ *(Rice et al 2001). Noda (2008)* uses physical arguments to argue that $V_{smax}$ is close to this limit of $c_s$, Since V must be smaller than $V_{smax}$ for the creep physics in eqn (2) to hold, and since we use this creep physics across all V, we shall henceforth use $\boldsymbol{V_{smax}}=0.5c_s$. However, we note that since $V_{smax}$ is under the *ln,* its exact value is probably not crucial.

**The contact diameter** *d* is taken as 1-15μm *(Beeler et al 2008).*

Thermal parameters are needed for eqns 5&6: From experiments at high slip rate, the **thermal equilibration distance,** $D_{th}$, is found to drop with applied normal stress, for all rock types, following an empirical relationship *(DiToro et al 2011)* where $D_{th}= k\,\sigma_n^{-q}$, and constants k and q depend on material. For lack of better constrains on k and q, we assume $k=5$ & $q=1$, which using the empirical relationship above predict $D_{th}$= 1m & 1cm at 5Mpa & 400MPa respectively, fitting on the one end results from 5MPa shear experiments on novaculite (Fig 2 of *DiToro et al 2004*) and at the other end providing $D_{th}$ of order of 1cm at $\sigma_n$ >200MPa (*DiToro et al, 2011*).

**Additional thermal parameters are C, ρ and α.** The thermal diffusivity for quartz is $\alpha = 7\ 10^{-6}\ m^2/s$ at room temperature, however existence of fault and gouge zone porosity reduces this diffusivity by up to an order of magnitude (*Gibert and Mainprice 2009, their fig 8; SimanTov et al 2015*). In addition, $\alpha$ drops with temperature *(Vosteen & Schellschmidt, 2003),* while the heat capacity, *C*, increases. We fit the thermal dependence of α of quartzite from *Hanley et al (1978)* (their fig 4). We then assume 1 order of magnitude reduction in α due to porosity in the fault zone (see Table 1 for equation). Density, $\rho$, is taken constant *(Vosteen & Schellschmidt 2003).* Table 1 reports the equation we fitted to the *C* variation with temperature shown in *Vosteen & Schellschmidt (2003*). Another parameter is the melting temperature, $T_m$, which for quartzite is ~ 1670C. *Rice (2006)* uses a "weakening temperature" which could be equated with $T_m$, yet suggests it is lower than melting, 1000-1400C, representing weakening due to "pre-melting". We consider all these values in our various calculations.

**Table 1 – table of parameters, definitions and values.**

| parameter | symb | Values | units | ref |
|---|---|---|---|---|
| volumetric activation volume | $\Omega_v$ | $(5 - 7.8) *10^{-29}$ | $m^3$ | Nakatani 2001, Rice 2001 |
| surface activation volum | $\Omega_s$ | $(5 - 7.8) *10^{-29}$ | $m^3$ | Nakatani 2001, Rice 2001 |
| Volumetric activation energy | $Q_v$ | 150- 280 | KJ/mol | Nakatani 2001, Rice 2001, Mainprice & Jaoul 2009 |
| Surface activation energy | $Q_s$ | 150- 280 | KJ/mol | Nakatani 2001, Rice 2001, Mainprice & Jaoul 2009 |
| Prefactor | B | 0.75-0.9 | - | here |
| ntact diameter | d | $1\text{-}15*10^{-6}$ | m | Beeler et al 2008 |
| Maximum shear rate | $V_{smax}$ | here 0.5 $c_s$ | | Noda 2008, Rice 2001 |
| Shear wave velocity | $c_s$ | 3750 | m/s | www.quartz.com |
| Reference cutoff time, room T | $t_{cr}$ | $10^0\text{-}10^6$ | s | Dieterich 1972, 1978, Nakatni & Scholz 2004a |
| cutoff time | $t_c$ | | s | from eqn 3 |
| activation energy for $t_c$ | $E_{tc}$ | 20-75 (calculated by | KJ/mol | Nakatani &Scholz 2004a |

| | | | | |
|---|---|---|---|---|
| | | eqn 3c) | | |
| Thermal equilibration distance. | $D_{th}$ | $=k\sigma_n^q$, here assume k=5, q =-1. | m | DiToro et al 2010, 2004 |
| (pre) melting temperatur | $T_m$ | 1270-1670 | K | Rice 2006 |
| Ambient temperature | $T_0$ | 300 | K | imposed |
| Heat capacity | C | $730*(1.7-200/T_c)$ | J/kg/K | Fitting fig 4 of Vosteen & Schellschmidt 2003 |
| Thermal diffusivity | $\alpha$. | $= \alpha_0*10^{-4}/T_c - 0.5*10^{-7}$; $\alpha_0=0.8$-5 | $m^2/s$ | fitting Fig4 of Hanley et al, 1978, assuming 1 order of magnitude reduction of $\alpha$ by porosity |
| Density | $\rho$ | 2650 | $Kg/m^3$ | |
| Contact temperature | Tc | 300-2000 | K | Calculated from eq 5 |
| Shear rate | V | $10^{-12}$-10 | m/s | Imposed. |
| Applied normal stress | $\sigma_n$ | 5 | MPa | Imposed |
| Steady-state friction coef | $\mu_{ss}$ | 0.01-1 | - | Calculated from eqn 3 |
| Contact shear stress | $\tau_c$ | (0.01-0.18) G | MPa | Calculated from eqn 3 |
| Contact normal stress | $\sigma_c$ | (0.1-0.22) G | MPa | Calculated from eqn 3 |
| Shear- prefactor | a | See Table 2 | - | Calculated from eqn 3 |
| Convergence- prefactor | b | See Table 2 | - | Calculated from eqn 3 |
| Avogadro number | N | $6 * 10^{23}$ | 1/mol | |
| Gas constant | R | 8.3 | J/mol/K | |
| Shear modulus | G | $31\ 10^9$ | Pa | |

## 4) Method

Although eqn (4b) provides a good approximation of steady-state friction at all velocity ranges, for accuracy we calculate friction from the primitive friction equation, eqn (4a). We solve equations (3), (4a), (5) &(6) numerically, seeking a coupled dynamic steady-state solution for contact stresses $\sigma_c$ and $\tau_c$ and contact temperature $T_c$, by iterative solutions using a Matlab subroutine that we wrote.

In our code the solution converges from the same reason that we propose a dynamic steady-state: Negative feedbacks ensure that steady-states in friction and temperature are coupled and are reached simultaneously. if $\tau_c$ rises it increases $T_c$ via shear heating (eqn 5). The increase in $T_c$ reduces $\tau_c$ via prefactor *a'*, in eqn (3d). The reduction in $\tau_c$ then reduces shear heating and so reduces $T_c$ in eqn (5). The reduced $T_c$ increases $\tau_c$ and so on.

An important deviation from this procedure is taken at high sliding velocity, when intense shear heating produces a steady-state $T_c$ that exceeds $T_m$. In this case eqn (6) gives contact stress, $\tau_c^m$, that maintains $T_c = T_m$ while sliding at velocity V. The present analysis uses velocity V ranging between $10^{-11}$ -10 m/s, calculating steady-state $T_c$, $\tau_c$, $\sigma_c$, and $\mu_{ss}$ as function of shear velocity V for sliding quartz, using 8 different combinations of material parameters, within the range stated in Table 1. All runs were run at room temperature, $T_0$=300K and normal stress $\sigma_n$=5Mpa. The parameters used for each of the runs are given in Table 2.

## 5) Results

**Contact temperature-** The first interesting result is the steady state contact temperature, $T_c$, versus sliding velocity, shown in Fig 4. All runs show three regimes of contact temperature behavior with similar transitions between regimes: at V smaller than a *critical thermal velocity* $V_t \sim 10^{-5}$ -$10^{-4}$ m/s, no substantial shear heating occurs, so $T_c \sim T_0$. For $V > V_t$, marked heating occurs. At a higher, second critical velocity, $V_m = 10^{-3}$ -$10^{-2}$ *m/s*, $T_c$ reaches $T_m$, the melting temperature. The very sudden and precipitous temperature rise at the contact scale between $V_t$ & $V_m$ explains why $V_m$ is essentially independent of the value of the melting temperature, $T_m$ (on a curve like that a difference in melting temperatures matters little), as seen by comparing runs 5&7, which have different $T_m$, yet similar $V_m$. The critical velocities, $V_t$ & $V_m$, depend primarily on thermal diffusivity and contact size: runs 1,3,6&8 show delayed onset of heating and melting due to small contacts and/or high thermal diffusivity (see Table 2).

**Table 2: summery of variables used in runs**. $a_r$ & $b_r$ stand for *a & b (*eqn 4) calculated at room temperature.

| **Run** | **1** | **2** | **3** | **4** | **5** | **6** | **7** | **8** |
|---|---|---|---|---|---|---|---|---|
| **Variable** | | | | | | | | |
| $\Omega_v(10^{-29}m^3)$ | 5 | 6.8 | 5 | 5 | 5 | 5 | 5 | 5 |
| $\Omega_s(10^{-29}m^3)$ | 6.8 | 6.0 | 7.8 | 7.8 | 7.8 | 6.8 | 7.8 | 7.8 |
| $Q_v$(KJ/mol) | 240 | 260 | 230 | 240 | 230 | 240 | 230 | 150 |
| $Q_s$(KJ/mol) | 260 | 210 | 280 | 270 | 280 | 260 | 280 | 185 |
| B | 0.8 | 0.9 | 0.9 | 0.89 | 0.9 | 0.8 | 0.9 | 0.75 |

| | | | | | | | | |
|---|---|---|---|---|---|---|---|---|
| $t_{cr}$(s) | $10^4$ | 2 | 1 | 2 | 1 | $10^4$ | 1 | $10^2$ |
| $T_m$(K) | 1270 | 1670 | 1270 | 1370 | 1670 | 1270 | 1270 | 1370 |
| $\alpha_0$ ($m^2$/s) | 1 | 1 | 2 | 1 | 1 | 2 | 0.8 | 1 |
| d ($\mu$m) | 1 | 10 | 1 | 10 | 10 | 1 | 15 | 3 |
| $a_r$ | 0.0085 | 0.0121 | 0.0077 | 0.0075 | 0.0077 | 0.0095 | 0.0077 | 0.0142 |
| $b_r$ | 0.0115 | 0.0108 | 0.0104 | 0.0094 | 0.0104 | 0.0129 | 0.0104 | 0.0233 |
| $a_r$ - $b_r$ | -0.003 | 0.0013 | -0.0027 | -0.002 | -0.0027 | -0.0034 | -0.0027 | -0.0091 |

**Contact stresses -** The combined effect of the parameters in Table 2, and the imposed slip rate *V* controls the value of contact scale stresses, $\tau_c$ & $\sigma_c$, shown in Fig 5.

The range of “play” in the values of the material parameters, especially the activation energies that may be differ by 100% between runs, and the value of B, which varies by 20% between runs, allows for a range of stress values to emerge, shifting curves up and down. Note the low values of $\tau_c$ & $\sigma_c$ in run8, due to the lower activation energies used in this run, representing the lower end of the allowed range (see Tables 1& 2).

Slip rate controls contact stresses both via simple velocity effects and via shear-heating effect on contact temperature: At low *V,* contact shear stress $\tau_c$ (Fig 5a) is always *velocity-strengthening* (abbreviated hereafter as *V-s*), due to the logarithmic *V-s* in eq(3b). However, once thermal effects kick in, for $V>V_t$ (see Fig 4), $\tau_c$ becomes *velocity –weakening*, abbreviated hereafter as *V-w*. *V-w* here is due to the increasing *a'* coefficient in eqn(3) that multiplies the negative log term. The linear increase of *a'* with $T_c$ overwhelms the log dependence on V. Melting onset, at $V=V_m$, occurs after a significant thermal softening already occurred in the regime $V_m>V>V_t$. For $V>V_m$ $\tau_c$ drops to compensate for the fact that $T_c$ is maintained at the constant $T_m$, following eqn 6.

The behavior of contact normal stress, $\sigma_c$, (Fig 5b), and the correlated real contact area $A_r$ (Fig 5c), is slightly different than that of $\tau_c$: $\sigma_c$ is *V*–s at very low *V.* The contact lifetime, $t=d/V$, decreases, hence the contact convergence and hence $A_r$ decreases with increasing V. The decreasing contact area increases $\sigma_c$. This trend continues as long as contact life time, *t,* is longer than the cutoff-time, $t_c$. Once the time contacts spend rubbing against each other is smaller than $t_c$, i.e once $t<t_c$, or in other words once $V>d/t_c$ (the theoretical prediction for this point is marked by arrows in Fig 5b), the logarithmic growth of contacts (eqns (3a) & (3c)) becomes negligible, and $\sigma_c$ saturates to $\sigma_c^0$. However, since $t_c$ is thermally activated, at $V>V_t$ shear heating may reduce $t_c$ (eq 3e). If $t_c$ decreases enough, it may become again smaller than contact lifetime $t$ (overwhelming the $t$ decrease that takes place with increasing $V$), so that the *log* term in eqns 3a again becomes significant, slightly reducing $\sigma_c$, a trend seen in runs 7,5,4, and 2. In our other runs the initial cutoff time at room temperature, $t_{cr,}$ was large, so $t_c$ didn't drop below $t$. As $V$ is increased further, melting is reached, and for $V>V_{m,}$ we assume $\sigma_c = const$, so that $\sigma_c$ saturates again.

**Friction coefficient-** The ratio between $\tau_c$ and $\sigma_c$ provides the steady state friction coefficient, $\mu_{ss,}$ as function of $V$, plotted in Fig 6. Our model predicts three or four main regimes of friction shown in Fig 6:

**1) At slow shear rate, when shear heating is negligible,** ($V< V_{t,}$) friction is either V-w or V-s, and follows R/S behavior. Whether friction is V-w or V-s in this regime depends on slight differences in parameter values: If contact normal stress, $\sigma_{c,}$ increases faster with $V$ than contact shear stress $\tau_c$ does, the resulting ratio $\tau_c/\sigma_c$ produces *V-w*, and vice versa.

This behavior can either extend up to $V=V_t$, or can in some cases transition to a sub-regime within the R/S regime. This sub-regime is characterized by a local *minimum of friction* within the R/S regime, at $V\sim d/t_c$. We term this value $d/t_c$ the *cutoff velocity* of the contact. Such a local minimum at $V\sim d/t_c$ is seen in Run8 of fig 6, with a zoom shown in fig 7. This is the behavior that produces the maximum in friction at intermediate V. It does not show much in DiToro et al data (our fig 1), but is common in various materials and under various conditions, as shown by *Bar Sinai et al (2014)*, and *Spagnuolo et al (2016)* (monzonite in their fig 2). This saddle-like behavior is analyzed in the Discussion section.

**3) At intermediate shear rate, $V_{melt}>V>V_t$,** shear heating softens *a', b'* and $t_c$ in eqn 3. This regime is always V- w, since $\tau_c$ (fig 5a) drops steeply with $V$, while $\sigma_c$ is only mildly V-w (fig 5b), if at all.

3) **At high shear rate, $V> V_{melt,}$** melting occurs, producing strong V-w, following eqn (6) , where $\tau_c$ drops as $1/\sqrt{V}$.

To summarize the results, the simulations from fig 6 are re-plotted in Fig 8 together with the experimental data for quartzose rocks from Fig 1 (from *DiToro et al, 2011*). The different model runs, which use a range of reasonable material parameters (as discussed in section 3, and summarized in Tables 1&2) predict and envelope the various behaviors observed experimentally in steady state sliding in quartz sandstone *(Dieterich, 1978),* granite *(Dieterich, 1978, DiToro et al 2004),* Tonalite and tonalitic cataclasite, *(DiToro et al 2006a),* and novaculite *(DiToro et al 2004, 2006b; Hirose and DiToro, unpublished, as reported in DiToro et al 2011).* Our model predicts:

1) The velocity weakening or velocity strengthening behaviors observed experimentally in the R/S regime.
2) In some cases, a minimum in friction occurs, followed by a peak.
3) The maximum peak in friction sometimes seen in experiments, here seen in the granite experiment of DiToro et al (2004) at V~ $10^{-4}$m/s. In the model the position of the peak depends on the parameters used. In particular, the peak is terminated at the velocity for onset of thermal-effects, $V_{t,}$ which is controlled mostly by thermal diffusivity and contact sizes, as explained above for Fig 4.
4) Abrupt thermal softening at V> $V_t$ ~$10^{-4}$ m/s. The transition to thermal softening is well fit by our model, as is the softening itself. Thermal softening is due to the efficient shear heating at V>$V_t$. $V_t$ is about 100 times smaller than the velocity required to cause melting of contacts ($V_m$). The transition to melting at $V_m$ continues the overall velocity weakening trend.

## 6) Discussion

The new model for steady-state friction is conceptually simple: it assumes thermally activated creep of contacts, under coupled steady-state stress and thermal conditions during sliding. The micro-mechanics model builds upon the works *of e.g. Putelet et al (2011), Rice et al (2001), Nakatani & Scholz (2004b), Bowden & Tabor (1964), Baumberger & Caroli (2006), Brechet & Estrin (1994)* and others, but adds thermal effects, relaxes the non-physical assumption of constant yield stress $\sigma_c^0$, and allows the activation energies and activation volumes to differ between shear and normal creep processes. The last assumption is crucial to capture the physics, as discussed at length below. We also added a physical constraint to represent melting, assuming that once contacts reach melting they reduce stresses to remain at $T_m$. Thus steady-state is still maintained during melting, which means the molten zone is not widening with slip. We are not clear that this is a good assumption, but the focus here is not on melting, so we leave this for future work.

## i. model results fit experiments well.

Since all parameters are obtained independently, or imposed externally, only a narrow 'play' range was left for model fitting. Despite rather tight constrains on parameters, our model fits well and explains friction under a large range of velocity, temperature and stress. In particular, we found a promising agreement between our simulations and:

1) Low temperature and normal stress experiments from tonalite, novaculite, quartz and granite (as complied by *DiToro et al 2011*). The fit using the range of parameters is seen in Fig 8.
2) High normal stress and low slip rate experiments on granite (*Blanpied et al, 1995)* that find a pronounced thermal weakening and strong positive slip-rate dependence above a critical temperature, see companion paper, Paper2.
3) A brittle-ductile transition that depends on slip rate and ambient temperature, as seen by *Chester and Higgs, (1992).* See companion paper, paper2.

## ii. The physics of friction as revealed by our model

The *a* & *b* pre-factors of eqn (4b) (which are the *a' & b'* of eqn (3) multiplied by $\mu_0$), have a definite physical interpretation in this model. The cutoff time also emerges as a physical parameter, which controls transitions between frictional regimes.

a) **<u>The *a* term:</u>** The $a\ ln(V/V_{smax})$ term arises from the $\tau_c$ equation*,* eqn 3b. This term is always negative since $V < V_{smax}$. Since at low velocities *a* is a positive constant and $ln(V/V_{smax})$ becomes less negative with increasing V, $\tau_c$ increases with V at low velocities, hence *we call this a term the viscous term*. At higher velocities, where $T_c$ increases*, a* also increases accordingly (eqn 4c), resulting in thermal–weakening of $\tau_c$, as explained below.

b) **<u>The *b* term</u>** is easier to understand in terms of the real area of contact rather than from $\sigma_c$. The $b\ ln(1+d/(Vt_c))$ in eqn (4b) is always positive, leading always to growth of real area of contacts. Thus *we call this b term the contact-area growth term.* Increasing $V$ reduces the growth of $A_r$ because the load lifetime on contacts is reduced. When $V >> d/t_c$, then $ln(1+d/Vt_c) \rightarrow 0$. An increase in $V$ however also increases $T_c$, with two effects: $T_c$ increases $b$, and decreases cutoff time $t_c$ (eqn 3d). The increase in $b$ is insignificant when $V >> d/t_c$, since it multiplies the *ln* term that is almost 0. Thus when $V >> d/t_c$ contact *Ar* & $\sigma_c$ are expected to saturate, as seen in Fig 5. A significant decrease in $t_c$ with increasing $T_c$ may however effect contact growth with increasing $V$ and by this slightly decrease $\sigma_c$ and increase *Ar* with increasing $V$ (see figs 5b & 5c). Whether significant enough reduction occurs in $t_c$ as $T_c$ increases, depends on the activation energy for $t_c$, which in turn depends on the process that occurs there, be it dislocation glide, stress corrosion, pressure solution or another creep process. For quartz our results suggest that the contact area growth term is only significant at slow V.

c) **The cutoff-time, $t_c$,** has a physical meaning that may be understood from evaluating the differential equation for contact normal stress, eqn (2c), at time t=0 and plugging in the definition of $t_c$ from eqn (2d), which gives:

$$\left.\frac{d\sigma_c}{dt}\right|_{t=0} = -b' \frac{\sigma_c^0}{t_c} \qquad (7)$$

Eqn (7) says that $t_c$ modulated by $b'$ is the combination of thermodynamic parameters, given by eqn (2e), that controls the characteristic time for contact convergence and growth, at the time of contact formation (t=0). Since $t_c$ is thermally activated (eqn 2e), the contact area growth rate, the rate of change in normal stress, and the rate of contact convergence are all thermally activated as well.

In addition to its physical meaning, the cutoff time is a crucial parameter in controlling transitions between friction-velocity regimes, as shown in *Ben David et al (1998*), and *Marone (1998*). This is also shown by our model (see discussion also in section 6.g): at slow sliding ($V<d/t_c$) contacts may grow significantly during their lifetime. At faster sliding contact area saturates. Thus, when sliding rate exceeds $d/t_c$, we expect a transition from *(a-b)* controlled friction to a friction that is controlled only by the *a* (viscous) parameter, and the *b* term to be negligible. It is shown below that $V=d/t_c$ indeed marks such a transition in the friction-velocity curve.

d) **Rate and state friction** is captured and predicted by our steady -sliding model. Our model, provided by eqn (4b), can be viewed as generalized R/S description, that should be coupled with steady-state contact temperature to predict the higher velocity friction. Eqn (1), the usual way that R/S is written in its steady-state form (e.g. *Scholz, 1998*), is obtained as the low-velocity limit of this generalized steady-state R/S, when $V<<d/t_c$. Under this approximation ln($1+\frac{d}{Vt_c}$) is approximated as ln($\frac{d}{Vt_c}$), the constants in eqn (4b) can be rearranged, and eqn (1) can be derived.

**e) The three slip regimes and the critical velocities:** Our simulations predict three sliding regimes as function of slip rate, where the transition between regimes is set by two, and sometimes three, critical slip rates, that mark transitions in behavior. The first critical velocity occurs at $V\sim d/t_c$, the "cutoff velocity" of the contact. When sliding faster than the cutoff velocity, contact growth is insignificant, and the b term is negligible. The 2nd critical velocity, $V_t$, is the velocity above which substantial shear-heating, and thus strong thermal weakening, takes place. The third critical slip rate is the one above which contacts melt, $V_m$. We find here that $V_t$ ranges between $10^{-5}$-$10^{-4}$ m/s, and $V_m$ ranges between $10^{-3}$-$10^{-1}$ m/s, depending on model parameters, mainly thermal diffusivity and contact size (see Fig 4 and Table 2). We next analyze friction dependence on velocity for these separate regimes.

**f) Slow sliding- The (a-b) term and the friction-velocity dependence:** Friction may be approximated in the slowest sliding regime, $V<<d/t_c$, by approximating ln($1+\frac{d}{Vt_c}$) as ln($\frac{d}{Vt_c}$). Then friction takes the form of eqn (1):

$$\text{(8a)}\quad \mu_{ss}\sim\mu_0 + a\ln\left(\frac{V}{V_{smax}}\right) - b\ln\left(\frac{Vt_c}{d}\right),$$

In this regime the two behaviors of R/S, namely V- weakening and V- strengthening, arise in our model when applying small differences in thermodynamic parameters, within the material-allowed range. The physics behind these two velocity dependencies are easily explained: Friction is the ratio of contact shear stress, $\tau_c$ and contact normal stress, $\sigma_c$. Since both $\tau_c$ and $\sigma_c$ increase logarithmically with slip rate in this regime (figure 5), V-w (or V-s) of friction arise when $\sigma_c$ increases with V slower (or faster) than $\tau_c$ does

(Fig 6). To see how V-s or V-w depend on material parameters, we calculate the dependence of $\mu_{ss}$ on V:

$$(8b)\ \frac{\partial \mu_{ss}}{\partial \ln(V)} = a - b = \mu_0 R T_c \left(\frac{1}{Q_s} - \frac{1}{BQ_v}\right)$$

where we used *a&b* from eqn (4c). Eqn (8b) predicts that when *(a-b)>0* friction is V-s, and when *(a-b)<0* friction is V-w. This prediction agrees with the standard interpretation of R/S laws *(Marone 1989),* and we term this regime the R/S regime. The predictions of eqn (8b) also agree with the observations of *Ikari et al (2011, 2016)* who find that (*a-b)* depends linearly on $\mu_0$ (note that although *Ikari et al* work on carbonates eqn (8b) is not material specific). In addition, in their Fig 2c, *Ikari et al (2016)* also find that *a & b* have different linear dependence on $\mu_0$, which according to eqn (4b) results from the difference in values between $Q_s$ & $BQ_v$. Eqn (8b) suggests that the difference between $Q_s$ & $BQ_v$ is a necessary condition for (*a-b)* to differ from 0, i.e. for V-s or V-w behavior to emerge. We stress that without a difference in activation energies and/or the existence of parameter B, (which ensures thermally activated $t_c$), the whole R/S behavior and also the possibility of a V-w sliding instability would not exist. Note also that eqn (8b) predicts a temperature dependence of *(a-b):* increasing temperature will enhance V-w by increasing the absolute value of *(a-b).* This prediction has implications for the depth of earthquake nucleation, which we shall leave for future studies. Table 2 calculates *a, b & a-b* at room T for each run.

**g. intermediate slip- the transition to velocity strengthening at V>> $d/t_c$.** The 2nd sliding regime emerges when the validity of the approximation in R/S eqn 8 breaks down, once V exceeds the cutoff velocity $d/t_c$. The break-down can be seen from Fig 6: Plugging the values of (a-b) from Table 2 in eqn 8, predicts that all runs in Fig 6 will be V-w, except for Run 2, that is predicted to be V-s, which it is. Yet, not all runs in fig 6 are V-w: runs 3, 6 & 8 are V-w at very low V, but transition to V-s, still within the low V regime, despite the fact that their *(a-b)<0* (i.e. despite $BQ_v - Q_s < 0$) . This transition from V-w to V-s is seen more clearly in the zoom into run 8, in fig 7, where a saddle-like behavior of friction is seen. The minimum in friction of runs 3, 6 & 8 arises when the condition under which eqn (8b) was derived is not met any more (the value of $d/t_c$ is indicated by arrows in fig 5b). Instead, for $V >> d/t_c$, one should approximate eqn (4b) by Taylor expanding $\ln(1+\frac{d}{Vt_c})$ as $\frac{d}{Vt_c}$, so that friction in this regime is:

$$(9a)\ \mu_{ss} \sim \mu_0 + a \ln\left(\frac{V}{V_{smax}}\right) + b\frac{d}{Vt_c},$$

The size of the *a & b* terms can be evaluated as follows: on the one hand for V<0.1 m/s $|\ln\left(\frac{V}{V_{smax}}\right)| \sim 10$, on the other hand, in this regime $\frac{d}{Vt_c} \ll 1$. Since *a* is of the same order as *b* (Table 2), then the *b* term in eqn 9a is negligible relative to the *a* term, and eqn (9a) can be approximated as

$$(9b)\ \mu_{ss} \sim \mu_0 + a \ln\left(\frac{V}{V_{smax}}\right)$$

Which means that contact growth is not important in this regime, as is also seen in Fig 5a&5c, which show contact stress and area saturate for V>> $d/t_c$.

In this regime, from eqn (9b), $\frac{\partial \mu_{ss}}{\partial \ln(V)} = a$, which is always positive. Thus *friction is always V-strengthening in this intermediate regime of* $V_t > V > d/t_c$ (I.e. sliding rate that is still slow enough to not cause appreciable shear heating effects), *independent of the sign of (a-b).* Physically this is because contacts don't have time to grow when the velocity exceeds the cutoff velocity $d/t_c$, and in absence of thermal effects (in this regime of still relatively slow slip), so only the logarithmic V-s of the viscous term of $\tau_c$ prevails. This regime however only exists under certain conditions. For example, runs 4,5 &7 don't show a V-s portion of the curve because the window between $d/t_c < V < V_t$ shrinks in these runs (they have small $t_c$, large *d,* and relatively small $V_t$).

Cases where this regime exists, as in run 8 (fig 7), show weakening at very low slip rate, followed by V-s at moderate slip rates (when $V > d/t_c$), and a transition to thermal softening at higher V, when $V > V_t$. A similar saddle-like behavior, causing a peak in friction, was experimentally observed in different materials (e.g. *Weeks and Tullis, 1985; Shimamoto, 1986; Kilgore et al., 1993; Heslot et al., 1994),* and its consequences have been discussed theoretically *(Noda 2008, Bar Sinai et al, 2014),* yet here we suggest the physics behind it. This issue of saddle-like behavior of friction, despite *a-b<0*, and despite relatively slow sliding (no shear heating yet) is important, as it reveals a basic behavior of friction that was largely overlooked in previous works. The saddle-like behavior of friction stems from the control of *d &* $t_c$ on a cutoff velocity, and may be overlooked if one concentrates solely on the sign of *a & b.*

**h. The thermal softening regime at $V>V_t$:** In the case of even faster slip rate, when V exceeds the thermal velocity $V_t$, the contacts heat up. At this fast velocity, certainly the condition of $V > d/t_c$ is met, and friction may be approximated by eqn 9b. But the derivative of friction is different now since it must include changes in temperature:

$$(10)\ \frac{\partial\mu_{ss}}{\partial V} \sim \frac{a}{V} + \frac{\partial a}{\partial V}\ln\left(\frac{V}{V_{smax}}\right) = \frac{a}{V} + \frac{\partial a}{\partial T_c}\frac{\partial T_c}{\partial V}\ln\left(\frac{V}{V_{smax}}\right)$$

$$= \frac{a}{V} + \frac{a}{V}\frac{T_c - T_0}{2T_c}\ln\left(\frac{V}{V_{smax}}\right)$$

To obtain the last term on the RHS we used $\frac{\partial T_c}{\partial V} = \frac{T_c - T_0}{2V}$ from eqn (5), and $\frac{\partial a}{\partial T_c} = \frac{a}{T_c}$ from eqn (4c). From the RHS expression in eqn (10) it is easy to see that friction thermally softens in this regime: the 1st term on the RHS is due to the regular velocity strengthening that is contributed by the viscous *a* term, and is always positive. The 2nd term on the RHS comes from thermal softening. It is negative and much larger than the 1st term, causing overall softening. This is easily seen by plugging values: e.g. for V=0.01m/s, $T_c \approx 250$C (Fig 4). Plugging $V_{smax}$ from Table 1 shows that the 2nd term is negative, with a magnitude that is 2.5 time the 1st term. In short, thermal softening occurs because the thermal effects of the *a* term overwhelm the velocity strengthening (viscous) effects of this *a* term.

**i. The melting regime at $V>V_m$:** when contacts melt, eqn 6 predicts that $\tau_c$ drops as $1/\sqrt{V}$. This is a consequence of the coupled steady-state calculation of T and stresses. This drop is slower than the $\tau_c \sim 1/V$ predicted by the flash melting model of *Rice 2006*. The difference is since the flash melting model does not be produce steady-state. At this point we can't say if steady-state is indeed achieved at melting conditions. However, since melting is not the main issue of this study, we simply state this difference.

## iii. Constraining the parameters:

The original B&T paper (1950) concluded that because friction is $\tau_c/\sigma_c$, the ratio of strength properties of the same material, the value of the friction coefficient should be independent of material. They also believed that $\tau_c$ & $\sigma_c$ both follow the same T dependence and so friction should be independent of T over a wide range of T. In geology the 1st conclusion is known as Byerlee's law, which applies to all geological materials except for the laminar materials like phylosilicates (as was also recognized by B&T, 1964, chapter XI), which have unusual frictional properties.

The 1st conclusion of B&T (1950) agrees with our prediction: $Q_s$, $BQ_v$, $\Omega_S$ & $\Omega_V$ determine $\mu_{ss}$ via $\tau_c$ & $\sigma_c$, and the absolute value of these depend on material. However, their ratio should depend mainly on process and not on material. We will discuss the ambient temperature effect on friction at low velocities (in relation to the B&T 2nd conclusion) in paper2.

We have constrained parameter values for our model based on thermodynamics measurements, as explained in section 3. Yet these parameters have a range of permissible values, as noted in Table 1&2 and seen in Figs 6&8. One may further constrain these parameters within the allowable range, using experiments of friction and velocity trends. For this we concentrate on the friction coefficient at the limit of slow V, V<<d/$t_c$, derived in eqn (8a). In this very slow velocity regime, friction is V-w if *(a-b)<0* , which requires $Q_s > BQ_v$. Since we know quartz is generally V- w, eqn 8 implies that in quartz the surface activation energy $Q_s$ should be larger than $BQ_v$, the volumetric activation energy multiplied by constant B. We used this constraint in all runs, except for run2 (which we added for exploratory purposes). Another constraint, discussed in section 3, is that $Q_v$ and $Q_s$ in quartz are constrained by independent measures reported in the literature to be between 150 and 280 KJ/mol.

One may constrain $Q_s$, B & $Q_v$ further, by using experimental data of steady-state values of *(a-b)*. *Marone (1998)* compiled experiments on bare rock and gouge and finds steady-state values of *(a-b)* for quartz, granite, and novaculite between 0 and -0.006. Since from eqn(4b) $(a-b) = \mu_0 R T_c \left(\frac{1}{Q_s} - \frac{1}{BQ_v}\right)$, this constrains the difference between 1/$Q_s$ and 1/($BQ_v$) to be at most -0.006/($\mu_0 R T_c$). Using room temperature, and assuming $\mu_0$ ~ 1, this constrains $\left(\frac{1}{Q_s} - \frac{1}{BQ_v}\right) \geq -2.4\ 10^{-6}$, which predicts $BQ_v \geq \frac{Q_s}{1+2.4\ 10^{-6} Q_s}$. We use this constraint in all runs expect for run8. Thus our runs show (*a-b*) values within the experimental range reported by *Marone (1998)* in all runs except run8, which has larger difference between $\left(\frac{1}{Q_s} - \frac{1}{BQ_v}\right)$ and so predicts a somewhat larger *(a-b)* (see Table 2).

An additional constraint is given by the value of the base friction $\mu_{base}$ (the part of friction that does not change with V), which is defined when we rewrite eqn (8a) as $\mu_{ss} \sim \mu_{base} + (a-b)\ln(V)$, with $\mu_{base} \sim \mu_0 + b\ln\left(\frac{d}{t_c}\right) - a\ln(V_{smax})$. The requirement that $\mu_{base}$ of quartz will be around 0.7-0.8 under slow sliding and room T, dictates a relationship between model parameters. In particular the fact that $a\&b$ are already constrained, as discussed in the previous paragraph, now dictates a relationship between $V_{smax}, t_c$ & $d$.

An additional check for the parameters of the model is offered by the value of the real contact area, as seen in Fig 5c. In agreement with the experiments of Kilgore and Dieterich (1994), we obtain that the value of the real contact area is about $10^{-3}$ of the nominal area at room temperature and low normal stress. The change of Ar with V, and its constancy for V exceeding $d/t_c$, can be tested in future experiments.

Finally, the parameters $\alpha_{therm}$ and $d$ are independently constrained, as discussed in section 3. However, they are checked by $V_t$, the velocity at which thermal weakening initiates. $V_t$ is observed by experiments (Fig8) to be around $10^{-4}$- $10^{-3.}$ This constrains the ratio $d/\alpha_{therm}$ from eqn(5), assuming we know $D_{th}$ from experiments.

**The importance of the difference between volume creep and shear creep.**

From section 6.ii.f and eqn 8, it is clear that the values and differences between $Q_s$ & $Q_v$, the activation energies that control contact convergence and surface shear respectively, are important for fault stability. The difference between shear and volume creep processes has not been dwelled upon previously, yet eqn 8 shows that it controls the V-s or V-w behavior of friction, and is essential for the emergence of R/S behavior. Such a differences in parameters may arise from different processes controlling contact growth and shear, or from variations in structure as function of distance from contact, as discussed in sec. 3. The values of $Q_s$ & $Q_v$ are not accurately known at present. Possible ways to measure separately Q (and $\Omega$) for surface and volume processes, involve micro-indentation hardness experiments at varying temperature to extract the $b$ dependence on $T_0$. $Q_v$ may then be extracted as function of t and T, following eqn (3a). One can also measure $a$ & $b$ as function of temperature to extract the activation energies, as in *Ikari et al (2011, 2016).* In that case fitted parameters at low V & T are used to model the full phase space, namely the non-monotonic friction as function of high V, T and $\sigma_n$. A good fit across the full phase space, as obtained here and in paper 2, lends confidence to the validity of the model.

## iv. Plastic vs brittle behavior of contacts

We have assumed that deformation at contacts, for what otherwise are considered brittle materials, is by low temperature plastic flow. Other models of rock friction have assumed brittle fracture at the contacts (e.g. *Beeler*, 2004). Such models produce similar results to ours because, as mentioned earlier, the velocity of sub-critical crack growth depends exponentially on stress, similar to our eqn. 2a. Our assumption of contact scale plasticity is based on the observation that for such materials, under static and moving loads, well-formed indentations and wear grooves are formed concordant with the indenting styli (*Brace*, 1963; *Engelder and Scholz*, 1976). This is explained because the high hydrostatic pressures that exist beneath contacts inhibits brittle fracture there (*Bowden and Tabor*, 1964 p.349; *Evans and Goetze*, 1979).

The wear detritus from rock friction is often dominated by angular fragments forming cataclasites. This indicates an important role for brittle fracture. The indentation experiments of *Brace (1963)* produced cone cracks surrounding the indents and in the sliding styli experiments of *Engelder and Scholz (1976)* partial cone cracks were observed at the trailing edge of the styli tracks. Such cone cracks are predicted by the high tensile stresses that exist at the edges of contacts [*Johnson*, 1985 p. 94; *Lawn*, 1967]. Thus, while plastic deformation at the contacts is the controlling process for friction, the growth of such cone cracks will lead to the plucking out of contacts, which will volumetrically dominate wear.

## Conclusions:

1. A physics-based model is proposed, based on the assumption of contact creep, to quantitatively predict steady-state friction. The steady state is both of contact temperature and stresses at contacts. The model generalizes R/S friction and finds its physical basis. The *a&b* parameters emerge as viscous & contact growth terms respectively.
2. The model explains and predicts the general observations of friction, that are not material specific:
    - A. High friction and 2nd order velocity dependence at low V (traditional R/S friction law behavior).
    - B. Material dependent peak at intermediate velocity, just before onset of thermal effects.

C. Abrupt weakening above a critical velocity, termed $V_t$ for thermal. At this velocity shear heating becomes meaningful. $V_t$ is ~100 times slower then the velocity that produces contact melting.

D. All material dependencies result from variations in material properties that may be independently determined.

3. R/S in its usual form, eqn (1), is shown to be the low-velocity limit of our model, representing an end-member behavior on a continuum of the same physical behavior. Our model predicts two more experimentally-observed regimes for frictional behavior, beyond the conventional R/S. The onset of the 2nd regime (this regime is not always present) is dictated by the cutoff time, $t_c$: When slip rate exceeds $d/t_c$, contacts cant grow appreciably during sliding. This leads to contact area saturation and velocity strengthening. This reveals the importance of the cutoff time $t_c$ for friction. The 3rd regime occurs at even faster sliding, when shear heating causes thermal softening. Thermal softening is achieved via thermal reduction of the viscous $a$ term.
4. The model predicts the importance of the difference between activation energies for shear and normal creep processes. The difference between these energies controls controls whether friction is velocity weakening or strengthening in the Rate &state regime.
5. Applicability of this model to high ambient temperature and stress will be demonstrated in paper2.

## Bibliography

1. Atkinson, B. K. (1987), Introduction to fracture mechanics and its geophysical applications, in Fracture Mechanics of Rock, edited by B. K. Atkinson, pp. 1-26, Academic Press, London.
2. Bar-Sinai, Y., Spatschek, R., Brener, E. A., and Bouchbinder, E. (2014). On the velocity-strengthening behavior of dry friction. JGR: Solid Earth, 119(3), 1738-1748.
3. Baumberger, T., 1997. Contact dynamics and friction at a solid-solid interface: material versus statistical aspects. Solid State Commun.102, 175–185.
4. Baumberger, T., & Caroli, C. (2006). Solid friction from stick–slip down to pinning and aging. Advances in Physics, 55(3-4), 279-348.
5. Beeler, N. M. (2004), Review of the physical basis of laboratory-derived relations for brittle failure and their implications for earthquake occurrence and earthquake nucleation, Pure and Applied Geophysics, 161(9-10), 1853-1876, doi:10.1007/s00024-004-2536-z.

6. Beeler, N. M., Tullis, T. E., & Goldsby, D. L. (2008). Constitutive relationships and physical basis of fault strength due to flash heating. JGR: Solid Earth (1978–2012), 113(B1).
7. Ben-David, O., Rubinstein, S. M., & Fineberg, J. (2010). Slip-stick and the evolution of frictional strength. Nature, 463(7277), 76-79.
8. Berthoud, P., Baumberger, T., G'sell, C., & Hiver, J. M. (1999). Physical analysis of the state-and rate-dependent friction law: Static friction. Physical review B, 59(22), 14313.
9. Boneh, Y., Sagy, A., & Reches, Z. (2013). Frictional strength and wear-rate of carbonate faults during high-velocity, steady-state sliding. EPSL, 381, 127-137.
10. Bowden, F. P., & Tabor, D. (1950). The friction and lubrication of solids (Vol. 1, No. 1). Oxford: Clarendon press.
11. Bowden, F. P., & Tabor, D. (1964). The friction and lubrication of solids (Vol. 2, No. 2). Oxford: Clarendon press.
12. Blanpied, M. L., Lockner, D. A., & Byerlee, J. D. (1995). Frictional slip of granite at hydrothermal conditions. JGR: Solid Earth (1978–2012), 100(B7), 13045-13064.
13. Brace, W. F. (1963), BEHAVIOR OF QUARTZ DURING INDENTATION, Journal of Geology, 71(5), 581-595.
14. Braeck, S., & Podladchikov, Y. Y. (2007). Spontaneous thermal runaway as an ultimate failure mechanism of materials. Physical Review Letters, 98(9), 095504.
15. Brechet, Y., Estrin, Y., (1994). The effect of strain rate sensitivity on dynamic friction of metals. Scripta Met. Mater. 30, 1449–1454.
16. Brown, K. M., & Fialko, Y. (2012). Melt-welt mechanism of extreme weakening of gabbro at seismic slip rates. Nature, 488(7413), 638-641.
17. Carpenter, B. M., Collettini, C., Viti, C., & Cavallo, A. (2016). The influence of normal stress and sliding velocity on the frictional behaviour of calcite at room temperature: insights from laboratory experiments and microstructural observations. Geophysical Journal International, 205(1), 548-561.
18. Chen, X., Madden, A. S., Bickmore, B. R., & Reches, Z. E. (2013). Dynamic weakening by nanoscale smoothing during high-velocity fault slip. Geology, 41(7), 739-742.
19. Chester, F. M. (1994). Effects of temperature on friction: Constitutive equations and experiments with quartz gouge. JGR: Solid Earth (1978–2012), 99(B4), 7247-7261.
20. Chester, F. M., and N. G. Higgs (1992), Multimechanism Friction Constitutive Model For Ultrafine Quartz Gouge At Hypocentral Conditions, JGR-Solid Earth, 97(B2), 1859-1870.
21. Del Gaudio, P., Di Toro, G., Han, R., Hirose, T., Nielsen, S., Shimamoto, T., & Cavallo, A. (2009). Frictional melting of peridotite and seismic slip. JGR: Solid Earth (1978–2012), 114(B6).

22. De Paola, N., Hirose, T., Mitchell, T., Di Toro, G., Viti, C., & Shimamoto, T. (2011). Fault lubrication and earthquake propagation in thermally unstable rocks. Geology, 39(1), 35-38.

23. De Paola, N., Holdsworth, R. E., Viti, C., Collettini, C., & Bullock, R. (2015). Can grain size sensitive flow lubricate faults during the initial stages of earthquake propagation? EPSL, 431, 48-58.

24. den Hartog, S. A., Peach, C. J., de Winter, D. M., Spiers, C. J., & Shimamoto, T. (2012). Frictional properties of megathrust fault gouges at low sliding velocities: New data on effects of normal stress and temperature. Journal of Structural Geology, 38, 156-171.

25. Dieterich, J. H. (1972), Time-dependent friction in rocks, J. Geophys. Res., 77, 3690–3697.

26. Dieterich, J. H. (1978). Time-dependent friction and the mechanics of stick-slip. Pure and applied geophysics, 116(4-5), 790-806.

27. Dieterich, J. H. (1979). Modeling of rock friction: 1. Experimental results and constitutive equations. JGR: Solid Earth (1978–2012), 84(B5), 2161-2168.

28. Dieterich, J. H., and B. D. Kilgore (1994), Direct observation of frictional contacts—New insights for state-dependent properties, Pure Appl. Geophys., 143(1-3), 283–302.

29. Dieterich, J. H., and B. Kilgore (1996), Implications of fault constitutive properties for earthquake prediction, Proc. Natl. Acad. Sci. USA, 93, 3787-3794.

30. Di Toro, G., Goldsby, D. L., & Tullis, T. E. (2004). Friction falls towards zero in quartz rock as slip velocity approaches seismic rates. Nature, 427(6973), 436-439.

31. Di Toro, G., Hirose, T. Nielsen, S., Pennacchioni, G. & Shimamoto, T. Natural and experimental evidence of melt lubrication of faults during earthquakes. Science 311, 647-649 (2006a).

32. Di Toro, G., Hirose, T., Nielsen, S., Shimamoto, T., (2006b). Relating high-velocity rock friction experiments to coseismic slip. In “Radiated Energy and the Physics of Faulting”, Eds. Abercrombie, R., McGarr, A., Di Toro, G., Kanamori, H., Geophysical Monograph Series Vol. 170 (American Geophysical Union, Washington, D.C.), pp. 121-134.

33. Di Toro, G., Han, R., Hirose, T., De Paola, N., Nielsen, S., Mizoguchi, K., ... & Shimamoto, T. (2011). Fault lubrication during earthquakes. Nature, 471(7339), 494-498.

34. Evans, B., & Goetze, C. (1979). The temperature variation of hardness of olivine and its implication for polycrystalline yield stress. JGR: Solid Earth (1978–2012), 84(B10), 5505-5524.

35. Evans, B. (1984). The effect of temperature and impurity content on indentation hardness of quartz. Journal of Geophysical Research: Solid Earth (1978–2012), 89(B6), 4213-4222.

36. Engelder, T., and C. H. Scholz (1976), The role of asperity indentation and ploughing in rock friction- II. Influence of relative hardness and normal load, Int. J. Rock Mech. Min. Sci. & Geomech., 13, 155-163.

37. Faulkner, D. R., T. M. Mitchell, J. Behnsen, T. Hirose, and T. Shimamoto (2011), Stuck in the mud? Earthquake nucleation and propagation through accretionary forearcs, Geophysical Research Letters, 38.

38. Ferri, F., Di Toro, G., Hirose, T. & Shimamoto, T. Evidences of thermal pressurization in high velocity friction experiments on smectite-rich gouges. Terra Nova, 22, 347-353 (2010).

39. Fondriest, M., Smith, S. A., Candela, T., Nielsen, S. B., Mair, K., & Di Toro, G. (2013). Mirror-like faults and power dissipation during earthquakes. Geology, 41(11), 1175-1178.

40. Gibert, B., & Mainprice, D. (2009). Effect of crystal preferred orientations on the thermal diffusivity of quartz polycrystalline aggregates at high temperature. Tectonophysics, 465(1), 150-163.

41. Goldsby, D. L., & T. E. Tullis (2002), Low frictional strength of quartz rocks at subseismic slip rates, Geophys. Res. Lett., 29(17), 1844, doi:10.1029/2002GL015240.

42. Goldsby, D. L., & Tullis, T. E. (2011). Flash heating leads to low frictional strength of crustal rocks at earthquake slip rates. Science, 334(6053), 216-218.

43. Goren, L., & Aharonov, E. (2007). Long runout landslides: The role of frictional heating and hydraulic diffusivity. GRL, 34(7).

44. Goren, L., & Aharonov, E. (2009). On the stability of landslides: a thermo-poro-elastic approach. Earth and Planetary Science Letters, 277(3), 365-372.

45. Goren, L., Aharonov, E., & Anders, M. H. (2010). The long runout of the Heart Mountain landslide: Heating, pressurization, and carbonate decomposition. JGR: Solid Earth, 115(B10).

46. Green II, H. W., Shi, F., Bozhilov, K., Xia, G., & Reches, Z. (2015). Phase transformation and nanometric flow cause extreme weakening during fault slip. Nature Geoscience, 8(6), 484-489.

47. Han, R., Shimamoto, T., Hirose, T., Ree, J. H., & Ando, J. I. (2007). Ultralow friction of carbonate faults caused by thermal decomposition. Science, 316(5826), 878-881.

48. Han, R., Hirose, T., & Shimamoto, T. (2010). Strong velocity weakening and powder lubrication of simulated carbonate faults at seismic slip rates. JGR: Solid Earth (1978–2012), 115(B3).

49. Hanley, E. J., Dewitt, D. P., & Roy, R. F. (1978). The thermal diffusivity of eight well-characterized rocks for the temperature range 300–1000 K. Engin. Geology, 12, 31-47.

50. Heslot, F., Baumberger, T., Perrin, B., Caroli, B., Caroli, C., 1994. Creep, stick-slip, and dry friction dynamics: experiments and a heuristic model. Phys.Rev.E 49, 4973–4988.

51. Hirose, T. & Bystricky M. Extreme dynamic weakening of faults during dehydration by coseismic shear heating. Geophys. Res. Lett. 34, doi:10.1029/2007GL030049 (2007).

52. Ikari, M. J., Marone, C., & Saffer, D. M. (2011). On the relation between fault strength and frictional stability. Geology, 39(1), 83-86.

53. Ikari, M. J., Carpenter, B. M., & Marone, C. (2016). A microphysical interpretation of rate□and state□dependent friction for fault gouge. Geochemistry, Geophysics, Geosystems.

54. Johnson, K. L. (1985), Contact Mechanics, Cambridge Univ. Press, Cambridge.

55. Kelemen, P. B., & Hirth, G. (2007). A periodic shear-heating mechanism for intermediate-depth earthquakes in the mantle. Nature, 446(7137), 787-790.

56. Kirby, S. H., & Kronenberg, A. K. (1987). Rheology of the lithosphere: selected topics. Reviews of Geophysics, 25(6), 1219-1244.

57. Kirkpatrick, J. D., Rowe, C. D., White, J. C., & Brodsky, E. E. (2013). Silica gel formation during fault slip: Evidence from the rock record. Geology, 41(9), 1015-1018.

58. Lawn, B. R. (1967), Partial cone crack formation in a brittle material loaded with a sliding spherical indenter, Proc. Roy. Soc. London, Ser. A 299, 307-316

59. Lockner, D. A., Summers, R., & Byerlee, J. D. (1986). Effects of temperature and sliding rate on frictional strength of granite. Pure and applied geophysics, 124(3), 445-469.

60. Mainprice D. & Jaoul O. (2009) A transmission electron microscopy study of experimentally deformed quartzite with different degrees of doping, Phys. Earth & Planet. Interiors 172, (2009) pp. 55–66.

61. Marone, C and Scholz, C. (1988). The depth of seismic faulting and the upper transition from stable to unstable slip regimes. Geophys. Res. Lett. 15, 621–624

62. Marone, C. (1998). Laboratory-derived friction laws and their application to seismic faulting. Annual Review of Earth and Planetary Sciences, 26(1), 643-696.

63. Marone, C. The effect of loading rate on static friction and the rate of fault healing during the earthquake cycle. Nature 391, 69–72 (1998).

64. Mizoguchi, K., Hirose, T., Shimamoto, T. & Fukuyama, E. Reconstruction of seismic faulting by high velocity friction experiments: An example of the 1995 Kobe earthquake, Geophys. Res. Lett. 34, L01308, doi:10.1029/2006GL02793 (2007).

65. Nakatani, M. (2001). Conceptual and physical clarification of rate and state friction: Frictional sliding as a thermally activated rheology. JGR: Solid Earth (1978–2012), 106(B7), 13347-13380.

66. Nakatani, M., & Scholz, C. H. (2004a). Frictional healing of quartz gouge under hydrothermal conditions: 1. Experimental evidence for solution transfer healing mechanism. JGR: Solid Earth (1978–2012), 109(B7).

67. Nakatani, M., & Scholz, C. H. (2004b). Frictional healing of quartz gouge under hydrothermal conditions: 2. Quantitative interpretation with a physical model. JGR: Solid Earth (1978–2012), 109(B7).

68. Nielsen, S., Di Toro, G., Hirose, T., & Shimamoto, T. (2008). Frictional melt and seismic slip. JGR: Solid Earth (1978–2012), 113(B1).

69. Noda, H. (2008). Frictional constitutive law at intermediate slip rates accounting for flash heating and thermally activated slip process. JGR: Solid Earth (1978–2012), 113(B9).

70. Noda, H., & Lapusta, N. (2013). Stable creeping fault segments can become destructive as a result of dynamic weakening. Nature, 493(7433), 518-521.

71. Platt, J. D., Brantut, N., & Rice, J. R. (2015). Strain localization driven by thermal decomposition during seismic shear. JGR: Solid Earth.

72. Platt, J. D., Rudnicki, J. W., & Rice, J. R. (2014). Stability and localization of rapid shear in fluid□saturated fault gouge: 2. Localized zone width and strength evolution. JGR: Solid Earth, 119(5), 4334-4359.

73. Poirier, J. P. (1985). Creep of crystals: high-temperature deformation processes in metals, ceramics and minerals. Cambridge University Press.

74. Proctor, B. P., Mitchell, T. M., Hirth, G., Goldsby, D., Zorzi, F., Platt, J. D., & Di Toro, G. (2014). Dynamic weakening of serpentinite gouges and bare surfaces at seismic slip rates. Journal of Geophysical Research: Solid Earth, 119(11), 8107-8131.

75. Putelat, T., Dawes, J. H., & Willis, J. R. (2011). On the microphysical foundations of rate-and-state friction. Journal of the Mechanics and Physics of Solids, 59(5), 1062-1075.

76. Reches, Z. E., & Lockner, D. A. (2010). Fault weakening and earthquake instability by powder lubrication. Nature, 467(7314), 452-455.

77. Rice, J. R., Lapusta, N., & Ranjith, K. (2001). Rate and state dependent friction and the stability of sliding between elastically deformable solids. Journal of the Mechanics and Physics of Solids, 49(9), 1865-1898.

78. Rice, J. R. (2006). Heating and weakening of faults during earthquake slip. JGR: Solid Earth (1978–2012), 111(B5).

79. Ruina, A. (1983). Slip instability and state variable friction laws. JGR, 88(10), 359-10.

80. Rubinstein, S. M., Cohen, G., & Fineberg, J. (2004). Detachment fronts and the onset of dynamic friction. Nature, 430(7003), 1005-1009.

81. Scholz, C. H. (1972), Static fatigue of quartz, JGR., 77, 2104-2114.

82. Scholz, C. H. (1988) The brittle-plastic transition and the depth of seismic faulting. Geol. Rundsch. 77, 319–328.

83. Scholz, C. H. (1998). Earthquakes and friction laws. Nature, 391(6662), 37-42.

84. Scholz, C. H. (2002). The mechanics of earthquakes and faulting. Cambridge university press.

85. Scholz, C. H., and T. Engelder (1976), Role of asperity indentation and ploughing in rock friction, Int. J. Rock Mech. Min. Sci., 13, 149-154.

86. Scholz, C. H., P. Molnar, and T. Johnson (1972), Detailed Studies of Frictional Sliding of Granite and Implications for Earthquake Mechanism, Journal of Geophysical Research, 77(32), 6392.

87. Siman-Tov, S., Aharonov, E., Sagy, A., & Emmanuel, S. (2013). Nanograins form carbonate fault mirrors. Geology, 41(6), 703-706.

88. Siman-Tov, S., Aharonov, E., Boneh, Y., & Reches, Z. E. (2015). Fault mirrors along carbonate faults: Formation and destruction during shear experiments. Earth and Planetary Science Letters, 430, 367-376.

89. Shimamoto, T., & Noda, H. (2014). A friction to flow constitutive law and its application to a 2-D modeling of earthquakes. JGR: Solid Earth, 119(11), 8089-8106.

90. Shimamoto, T. (1986). Transition between frictional slip and ductile flow for halite shear zones at room temperature. Science, 231(4739), 711-714.

91. Spagnuolo E., S. Nielsen, M. Violay, G. Di Toro (2016), An empirically-based steady-state friction law and implications for fault stability, GRL, doi: 10.1002/2016GL067881

92. Stachowiak, G., & Batchelor, A. W. (2013). Engineering tribology. Butterworth-Heinemann.

93. Sulem, J., & Famin, V. (2009). Thermal decomposition of carbonates in fault zones: Slip-weakening and temperature-limiting effects. JGR: Solid Earth (1978–2012), 114(B3).

94. Tsenn, M. C., & Carter, N. L. (1987). Upper limits of power law creep of rocks. Tectonophysics, 136(1), 1-26.

95. Van Diggelen, E. W., De Bresser, J. H., Peach, C. J., & Spiers, C. J. (2010). High shear strain behaviour of synthetic muscovite fault gouges under hydrothermal conditions. Journal of Structural Geology, 32(11), 1685-1700.

96. Verberne, B. A., Spiers, C. J., Niemeijer, A. R., De Bresser, J. H. P., De Winter, D. A. M., & Plümper, O. (2014a). Frictional properties and microstructure of calcite-rich fault gouges sheared at sub-seismic sliding velocities. Pure Appl. Geophs, 171(10), 2617-2640.

97. Verberne, B. A., Plümper, O., de Winter, D. M., & Spiers, C. J. (2014b). Superplastic nanofibrous slip zones control seismogenic fault friction. Science, 346(6215), 1342-1344.

98. Verberne, B. A., Niemeijer, A. R., De Bresser, J. H., & Spiers, C. J. (2015). Mechanical behavior and microstructure of simulated calcite fault gouge sheared at 20-600° C: Implications for natural faults in limestone. JGR Solid Earth.

99. Vosteen, H. D., & Schellschmidt, R. (2003). Influence of temperature on thermal conductivity, thermal capacity and thermal diffusivity for different types of rock. Physics and Chemistry of the Earth, Parts A/B/C, 28(9), 499-509.

100. Weeks, J. D., & Tullis, T. E. (1985). Frictional sliding of dolomite: A variation in constitutive behavior. Journal of Geophysical Research: Solid Earth, 90(B9), 7821-7826.

101. Yao, L., Ma, S., Niemeijer, A. R., Shimamoto, T., & Platt, J. D. (2016). Is frictional heating needed to cause dramatic weakening of nanoparticle gouge during seismic slip? Insights from friction experiments with variable thermal evolutions. Geophysical Research Letters, 43(13), 6852-6860.

# Figures

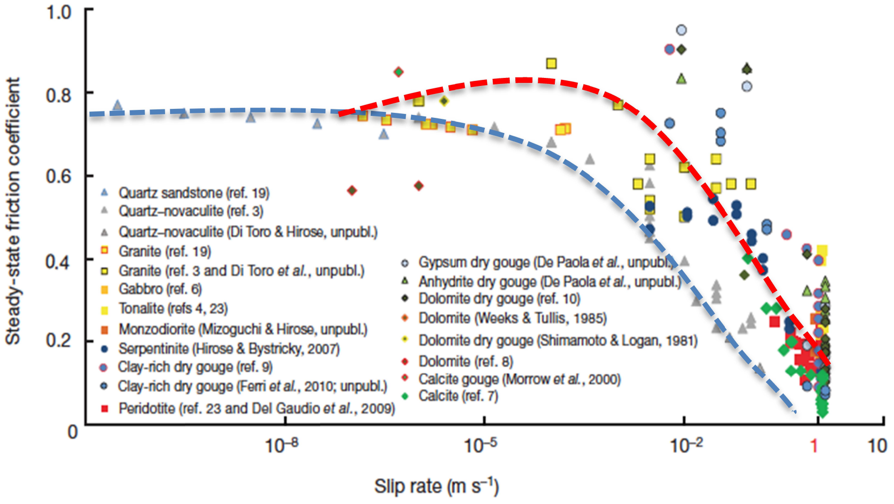

Fig 1: Steady-state friction, $\mu_{ss}$, as function of shear velocity, V, in experimental shear in various rocks, adapted from Fig 3 in DiToro et al, (2011). At slow shearing rate, $\mu_{ss}$ is high and varies only slightly with V. When V is greater than ~ cm/s, $\mu_{ss}$ starts to decrease strongly with increasing V for all rock and mineral types. Two curves are fit to the data, one with a peak at intermediate V, and another without. Different minerals behave in these two manners.

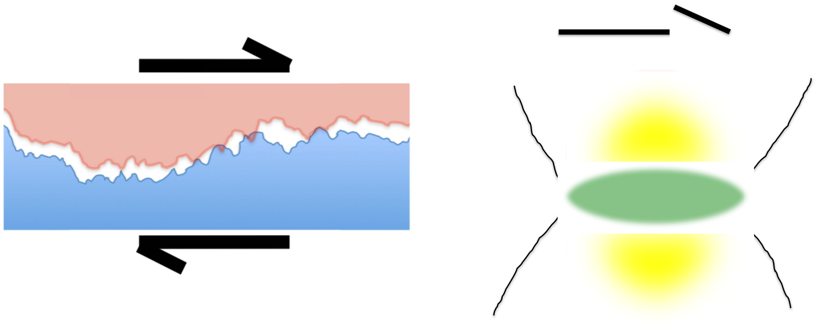

**Fig 2.** a) Illustration of shearing rough surfaces, depicting that the real contact area, $A_{r,}$ is much smaller than the apparent area of contact. b) Zoom into a single asperity contact. The red fuzzy area depicts a highly compressed region that may undergo volumetric creep, with a maximum depicted in yellow. This creep, driven by normal stress, may occur by dislocation glide within this region, pressure solution, or subcritical fracture growth, causing asperity convergence compensated by contact area growth. In contrast, the green region demarcates the contact interface, where shear-activated creep is localized. Note that the two creep processes may be different and that this difference strongly effects friction.

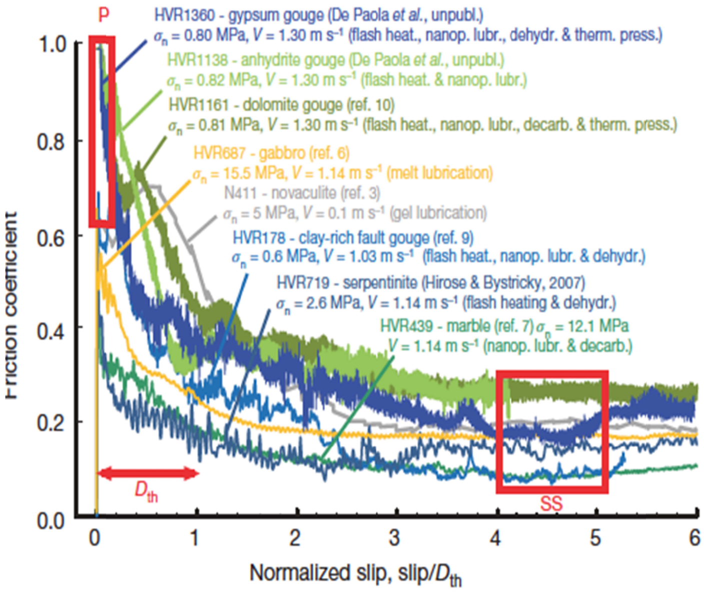

Fig 3. Di Toro et al (2011), their Fig 1, shows that independent of rock type, all rocks and gouge show similar weakening when sheared at high slip rate, and achievement of steady-state friction, after sliding a few characteristic thermal distances $D_{th}$.

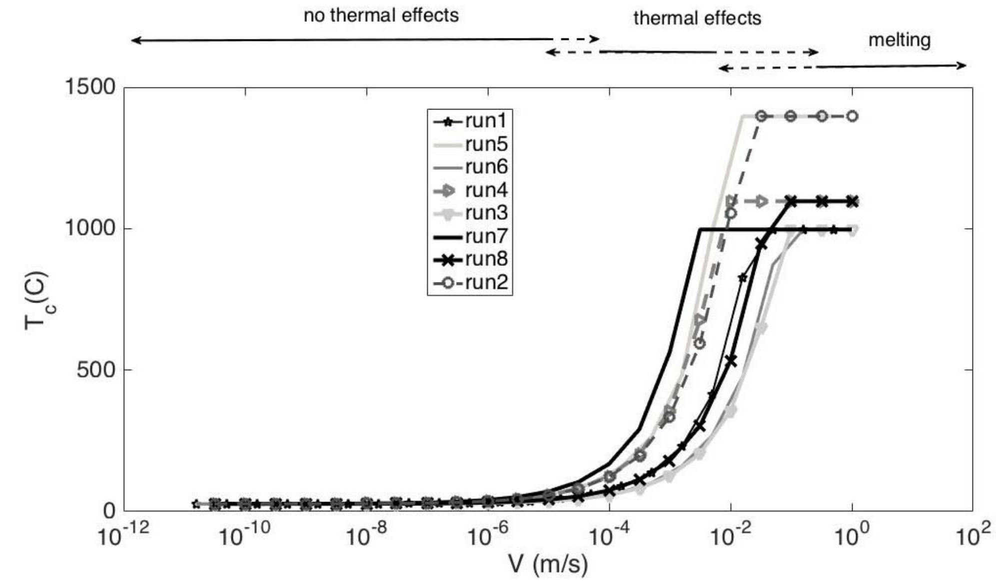

Fig 4: Our model calculated steady -state contact temperature ($T_c$) for quartz/granite sliding at room temperature and $\sigma_n$=5Mpa, as function of slip rate V. We present 8 runs, each using different parameter values within the independently predicted range (see Table 2). For low V, $T_c$ remains at $T_{0,}$ the ambient T. Increasing V brings about two transitions: at $V_t$ & at $V_m$. $V_t$ is the velocity at which marked heating begins, ~$10^{-4}$ m/s. At $V_m$, which varies between $10^{-3}$-$10^{-1}$ m/s, contacts reach melting temperature, $T_m$, capping the curves at $T_c$= $T_m$ for any V> $V_m$. The values of the transition velocities $V_t$ & $V_m$ depend primarily on thermal diffusivity and contact size: $V_t$ and $V_m$ in runs 1,3,6&8 are high since these runs have small contacts and/or high diffusivity. Note that runs 5,8,4 &2 used higher $T_m$, to illustrate the negligible effect the the value of $T_m$ has on $V_t$ & $V_m$.

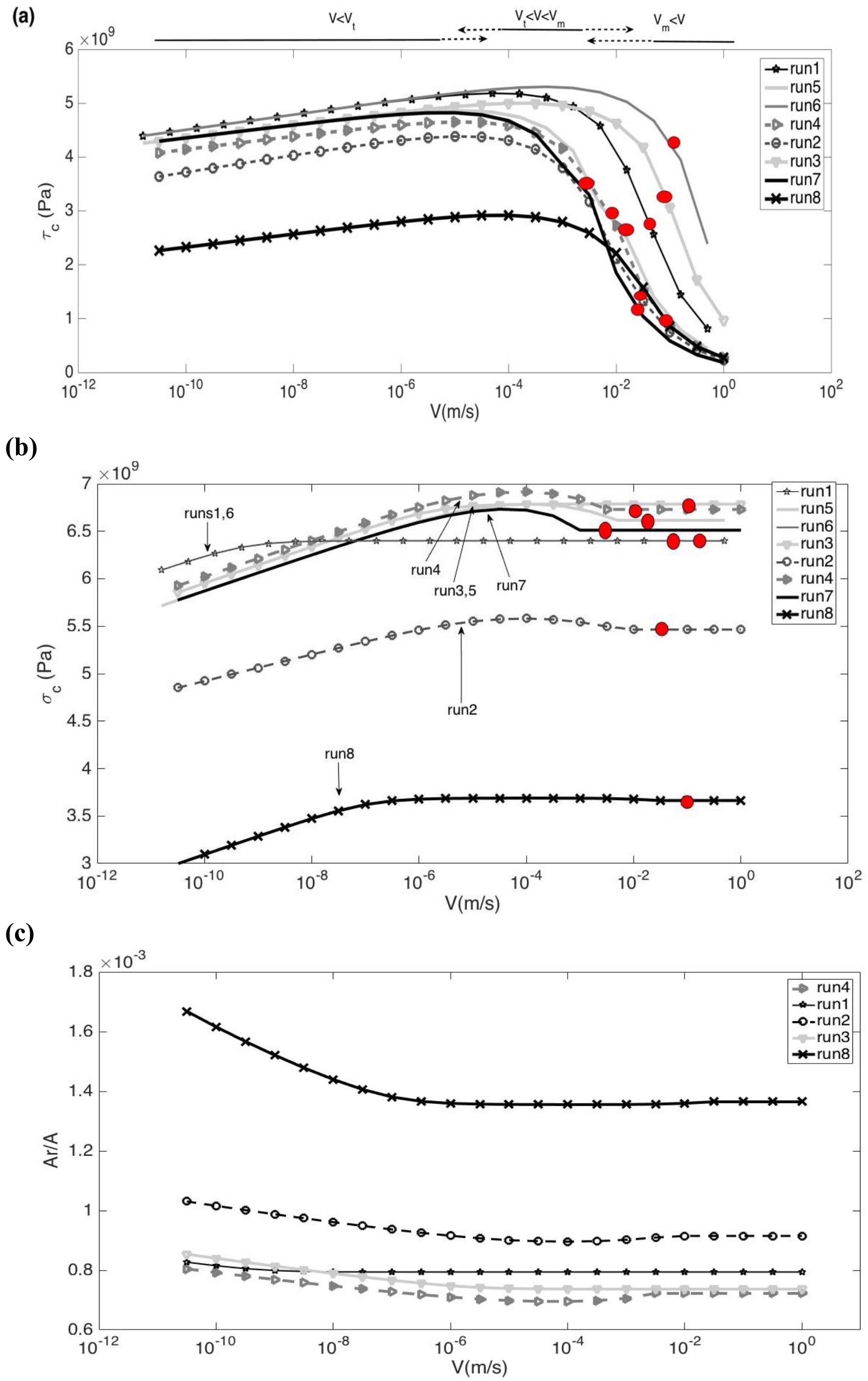

Fig 5: Contact shear, $\tau_c$, (a) and normal stress, $\sigma_c$ (b) as function of *V*, at $T_0$*=30C*, $\sigma_n$*=5Mpa.* Onset of melting marked by red circles. (**a**) For $V < V_t$ (~$10^{-5}$-$10^{-4}$ m/s), $\tau_c$ is *V-strengthening* in

all runs due to the log term in eq (3b). For V > $V_t$, $\tau_c$ becomes strongly *V-weakening* since thermal effects on coef *a* override the *V-strengthening* of the log term in eq (3b) (see also discussion and eqn 10). After melting $\tau_c$ continues to drop. **(b)** At low V, $\sigma_c$ is *V-strengthening* due to the increasingly limited time for contact growth during sliding (eq 3a). *V-strengthening* continues as long as contact life time, *t=d/V*, exceeds the cutoff time, $t_c$. At V > $d/t_c$ (this point marked by arrows for each curve), contact lifetime is smaller than $t_c$, so the *log* term in eq 3 becomes negligible, and $\sigma_c$ saturates. Constant $\sigma_c$ prevails unless shear heating reduces $t_c$ enough to make again $t > t_c$. If this occurs, $\sigma_c$ becomes *V-weakening*, as in curves 7,5,4, and 2. After melting $\sigma_c$ is assumed in the model to saturate and become constant. **(c)** Real contact area (normalized by nominal contact area) changes appreciably only for slow V, and remains constant at V>> $d/t_c$. At this point the b term becomes negligible (see eqn 9).

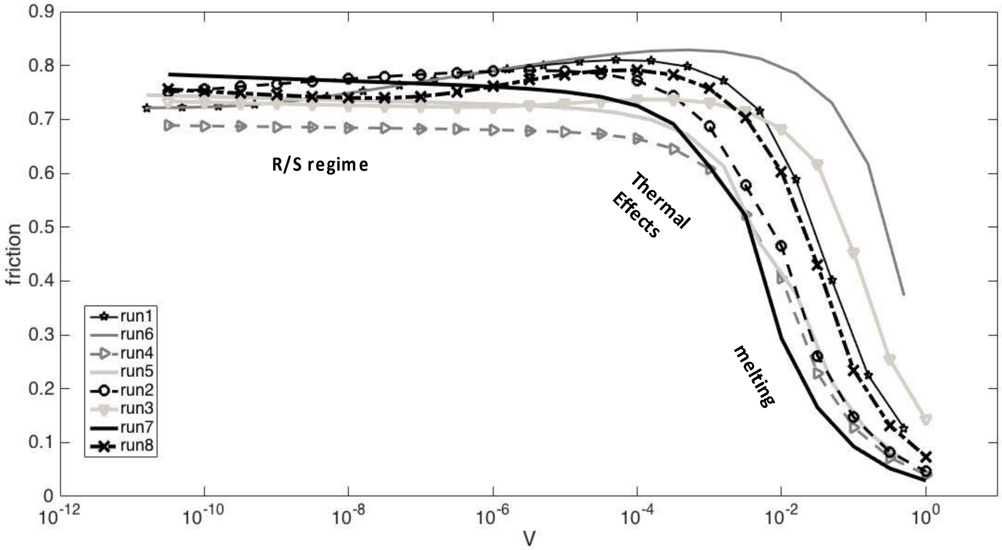

Fig 6: model predictions for steady-state friction coefficient, $\mu_{ss}$, in quartz and granite as function of slip-rate, *V,* for all runs in Table 2. Three main regimes of behavior are seen: At low *V* ($V<V_t$, where $V_t$ is thermal velocity, blue region), $\mu_{ss}$, is temperature-independent and follows the traditional rate and state behavior (R/S). Here $\mu_{ss}$ may be either V-weakening or V-strengthening, depending on small variations in thermodynamic parameters. At high enough *V* ($V_t<V<V_m$, where $V_m$ stands for melting velocity, yellow region), thermal effects kick in (see Fig 4), causing a marked V-weakening of friction. In some parameter regimes (e.g runs 3 &8), thermal-weakening is preceded by a friction minimum followed by a peak in friction, as observed sometimes in experiments (Fig 1). Fig 7 zooms into this regime in run8. At high V (red region) a transition to contact melting occurs (Fig 4), with further friction reduction.

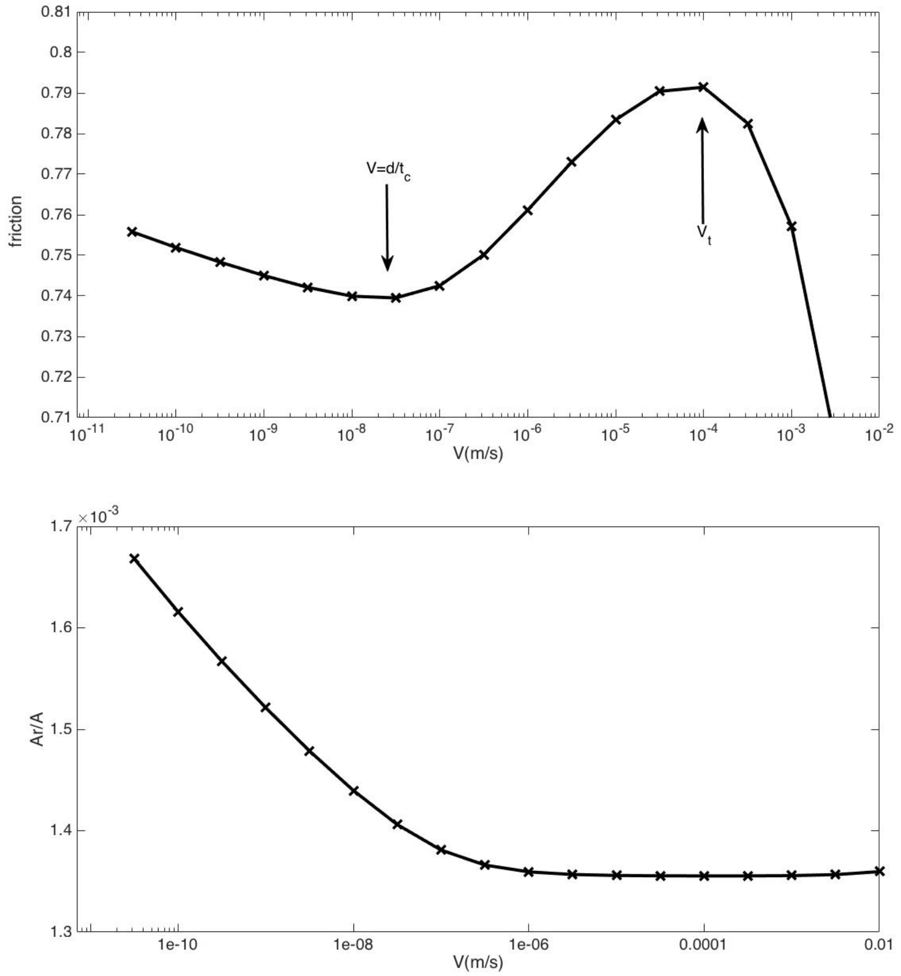

fig 7. Friction and real contact area from Run 8. This run exemplifies a situation when velocity weakening at geological slip rates, due to a-b<0, transitions to velocity strengthening at slightly higher slip rates (when $V>d/t_c$), due to the role that $t_c$ plays in the velocity dependence of $\mu_{ss}$.

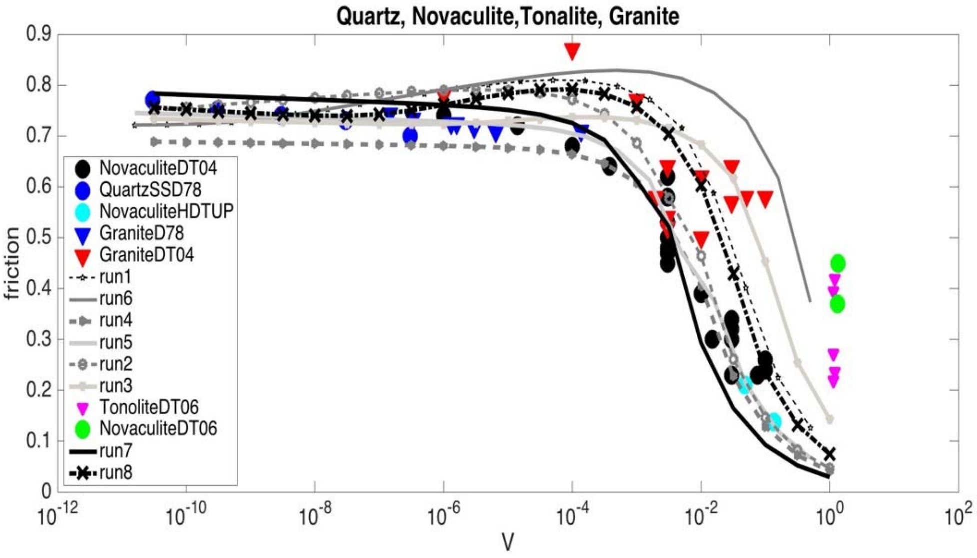

Fig 8: Our modeling results for steady-state friction, re-plotted from Fig 6, but now overlaid on top of the quartz sandstone, granite, novaculite & tonalite experimental results that were presented in Fig 1 (from DiToro et al 2011). Our physics-based model results show excellent fit to experiments at all velocities, and even predict the friction peak that is observed in some cases before the onset of melting. Experimental data (in symbols) is from shear experiments in Tonalite and tonalitic cataclasite (DiToro et al 2006a), Novaculite (DiToro et al 2004, 2006b; Hirose and DiToro, unpublished, reported in DiToro et al 2011), quartz sandstone (Dieterich, 1978), and granite (Dieterich, 1978, DiToro et al 2004).